CHAPTER 4

Results and discussion

Contents

4.1 Introduction

In this chapter the results from the spectroscopic and photometric studies are presented and discussed. The spectral emission diagrams (SEDs) of five stars that showed an Hα emission line are presented and discussed. The respective colour-colour and colour-magnitude diagrams follow. On each of the photometric diagrams the stars that showed Hα emission and were detectable with that specific filter are indicated.

The location of sources that matched in different optical filters are shown as an overlay for the NIR sources from the study done by de Villiers (2009). By matching up the optical and NIR sources, two-colour NIR diagrams could be constructed for the sources that were detected in specific optical filters. The clustering of young sources in the bubble region found by Van der Walt et al. (2012) is briefly discussed.

4.2 Spectroscopic results

4.2.1 Introduction

During the week of 15-19 February 2002, 24 stars were observed with the 1.9-m telescope at the SAAO. The 24 stars consisted of a selection of the brightest stars across the $7' \times 7'$ field of view centred on the methanol maser close to RCW 34. The spectral profiles, and a diagram of the location of the 24 stars, are given in appendix D. Of the 24 stars, two showed Hα emission lines.

From the NIR study conducted by de Villiers (2009) and the optical photometry, a list of possible candidates for a second set of observations could be compiled. The list of candidate stars was compiled from the 174 stars that matched in the R, I, J, H and K filters. A candidate star had to be brighter than an apparent magnitude of 16.5, which was the sensitivity limit of the 1.9-m telescope. A list of 76 candidate stars was compiled.

The 76 candidates were sorted according to the value of their $J - H$ colours. The reason for this is that the accretion disk of a T Tauri star has the highest excess emission in the J filter. A diagram showing the location of the 76 candidates and the emission profiles of the 38 stars that were observed are given in appendix E.

For the 76 candidates, a limitation on the telescope time available resulted in the observation of only 38 stars. A list of these 38 stars is given in Table 4.1. Out of the 38 stars, three showed Hα emission lines.

4.2.2 The SEDs for the stars with an Hα emission line

In an attempt to classify the stars that showed an Hα emission line their SEDs were placed next to standard spectral types from the spectral library of Pickles (1998). The Pickles library is a collection of SEDs for all the standard spectral star types, and spans from 1150Å to 25000Å. This library is based on the MK spectral class system first published by Morgan et al. (1943). A summary of key characteristics for the 5 stars that each showed an Hα emission line, is shown in Table 4.2.

The SED of star A is shown in Fig 4.1. The continuum is placed on an arbitrary scale and axis to facilitate comparisons of its spectral profile with those of standard stars. Star A is compared to a K3V, K7V and M0V type star because the relative strengths of the absorption lines for each is the closest to that of star A. Another reason is that star A's continuum is featureless compared to the spectral profiles of standard stars. Hence those that had a continuum closest to that of star A were used, for example K7.

The blue part of the continuum has a flat profile, but the relative flux of star A starts to increase from the Hβ line towards longer wavelengths. This can either be excess emission from matter moving in magnetic tubules from the accretion disk onto the star's surface, or it can be a star with a low surface temperature.

Rad	Dec	$J-H$	$H-K$
134.10449	-43.09930	0.786 ± 0.042	0.579 ± 0.055
134.19235	-43.09019	0.785 ± 0.018	0.390 ± 0.023
134.15894	-43.11704	1.312 ± 0.014	0.446 ± 0.015
134.12987	-43.15465	1.264 ± 0.028	0.638 ± 0.025
134.18756	-43.13396	1.189 ± 0.017	0.446 ± 0.013
134.04158	-43.07336	1.160 ± 0.015	0.360 ± 0.020
134.02945	-43.14342	1.123 ± 0.017	0.408 ± 0.017
134.13199	-43.09892	1.014 ± 0.013	0.319 ± 0.020
134.03705	-43.04820	0.769 ± 0.014	0.314 ± 0.021
134.17583	-43.15486	0.726 ± 0.018	0.465 ± 0.032
134.04009	-43.07355	0.718 ± 0.011	0.266 ± 0.019
134.0527	-43.0326	0.786 ± 0.013	0.195 ± 0.017
134.09006	-43.05240	0.762 ± 0.045	0.407 ± 0.065
134.11231	-43.13211	0.654 ± 0.010	0.363 ± 0.021
134.05996	-43.11056	0.636 ± 0.010	0.307 ± 0.022
134.03999	-43.07267	0.631 ± 0.011	0.374 ± 0.026
134.15392	-43.13682	0.614 ± 0.011	0.306 ± 0.025
134.0361	-43.0596	0.583 ± 0.020	0.286 ± 0.030
134.03448	-43.05326	0.579 ± 0.009	0.277 ± 0.022
134.1496	-43.0598	0.575 ± .014	0.184 ± 0.023
134.05548	-43.08768	0.511 ± 0.011	0.313 ± 0.030
134.12323	-43.03746	0.704 ± 0.012	0.313 ± 0.023
134.07521	-43.10569	0.809 ± 0.011	0.425 ± 0.036
134.09021	-43.11628	0.674 ± 0.010	0.296 ± 0.029
134.05889	-43.12385	0.666 ± 0.019	0.448 ± 0.035
134.11880	-43.11145	0.834 ± 0.012	0.247 ± 0.028
134.16549	-43.12586	0.700 ± 0.084	0.308 ± 0.053
134.06094	-43.05985	0.669 ± 0.009	0.392 ± 0.032
134.03914	-43.05055	0.645 ± 0.010	0.293 ± 0.026
134.0804	-43.0960	0.510 ± 0.009	0.271 ± 0.024
134.04604	-43.12952	0.866 ± 0.013	0.446 ± 0.033
134.1648	-43.1239	0.863 ± 0.014	0.249 ± 0.009
134.18555	-43.13043	0.777 ± 0.018	0.341 ± 0.023
134.18504	-43.13958	0.735 ± 0.016	0.398 ± 0.028
134.03606	-43.10434	0.699 ± 0.010	0.449 ± 0.027
134.12315	-43.03826	0.820 ± 0.008	0.291 ± 0.024
134.10449	-43.09930	0.786 ± 0.042	0.579 ± 0.055
134.19235	-43.09019	0.785 ± 0.018	0.390 ± 0.023

Table 4.1: The 38 stars from which spectroscopic images were taken in 2011.

The three spectral types were plotted next to star A for the purposes of comparison. By considering at the continuum emission of late K type stars in Fig 4.1, it is readily apparent that star A has the same surface temperature as the others in the same spectral class.

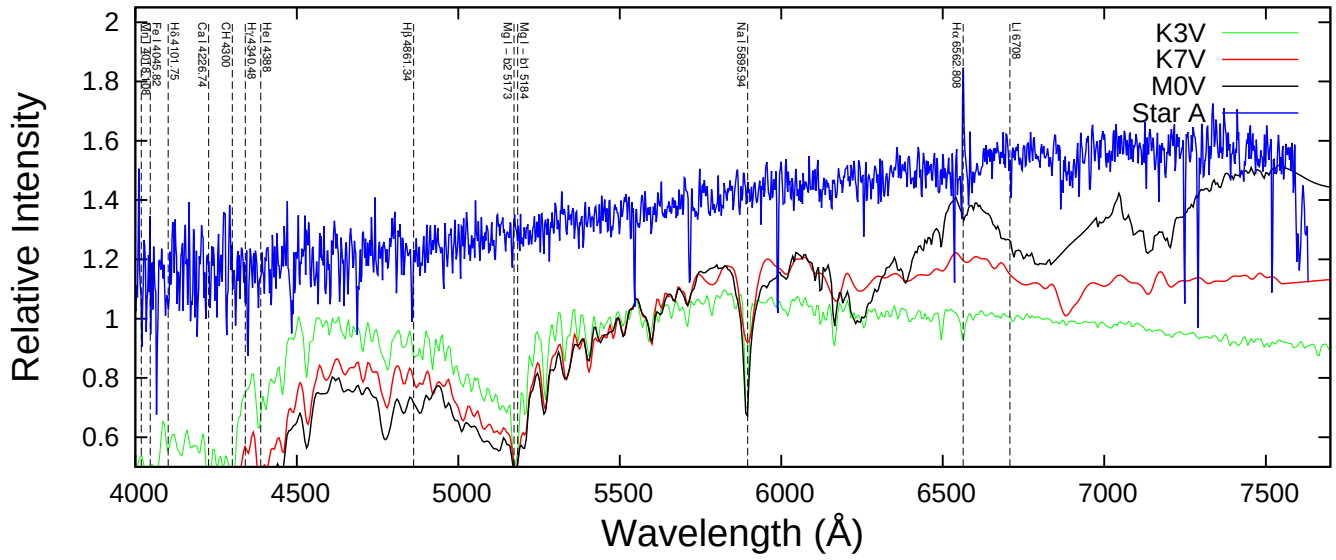

Figure 4.1: The spectral emission profile for star A.

Star A has a prominent Hα emission line which peaks at 6567 Å and has an asymmetric base towards the red side of the spectrum. The Hα line is caused by circumstellar matter, so it can either be from an accretion disk if it is a CTT or it can be due to strong coronal activity if it is a WTT.

The asymmetric base suggests that the matter causing the emission of the line is moving in opposite directions relative to each other. This may be matter rotating in the accretion disk at opposite ends of the star. The Hα emission line lies a bit towards the longer wavelength side of the indicator line. This is due to the wavelength calibration of the image that is incorrect within 4Å, so that all of the emission/absorption lines lie on values a few Angstrom larger than their actual values. This was corrected by subtracting 5Å from all of the wavelength values.

The Li absorption line ($\lambda \approx 6708$ Å) has an asymmetric profile, and is the strongest at 6715 Å. The Li absorption line is only found in very young PMS stars - this is a confirmation that there are young stars in the vicinity of RCW 34, as postulated by de Villiers (2009).

In Fig 4.2 the spectral profiles of star B, late K type stars and early M type stars are shown. The continuum of star B tends to follow the trend of these low mass stars. In both Figs 4.1 and 4.2 the spectra are very noisy. The blue part of a star's spectrum (from 4000Å-5000Å) is usually used to do spectral classification but it is unusable in all of the spectra. The reason for the low $\frac{S}{N}$ in the blue part of all of the spectra obtained in 2011 is that most of the sources were very faint - close to the limit of the 1.9-m telescope. And the CCD used has a very low effectivity at these wavelengths.

The Pickles spectral library was not used for the classification of stars C and D because they were not flux calibrated. Therefore, an alternative with normalised spectral profiles was used. A website

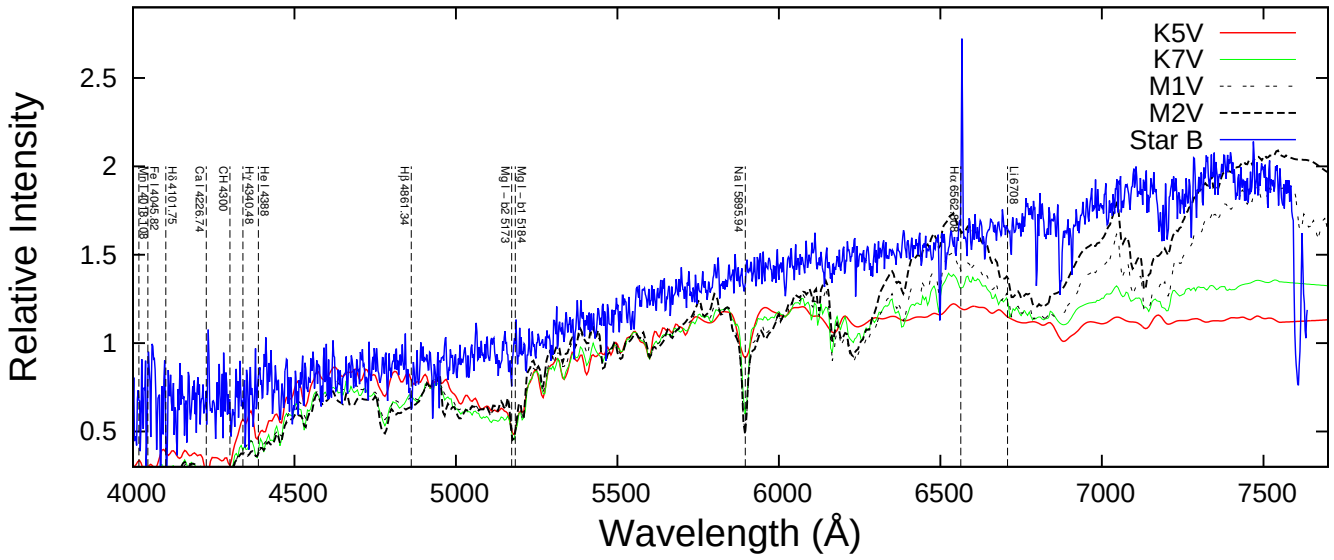

Figure 4.2: The spectral emission profile for star B.

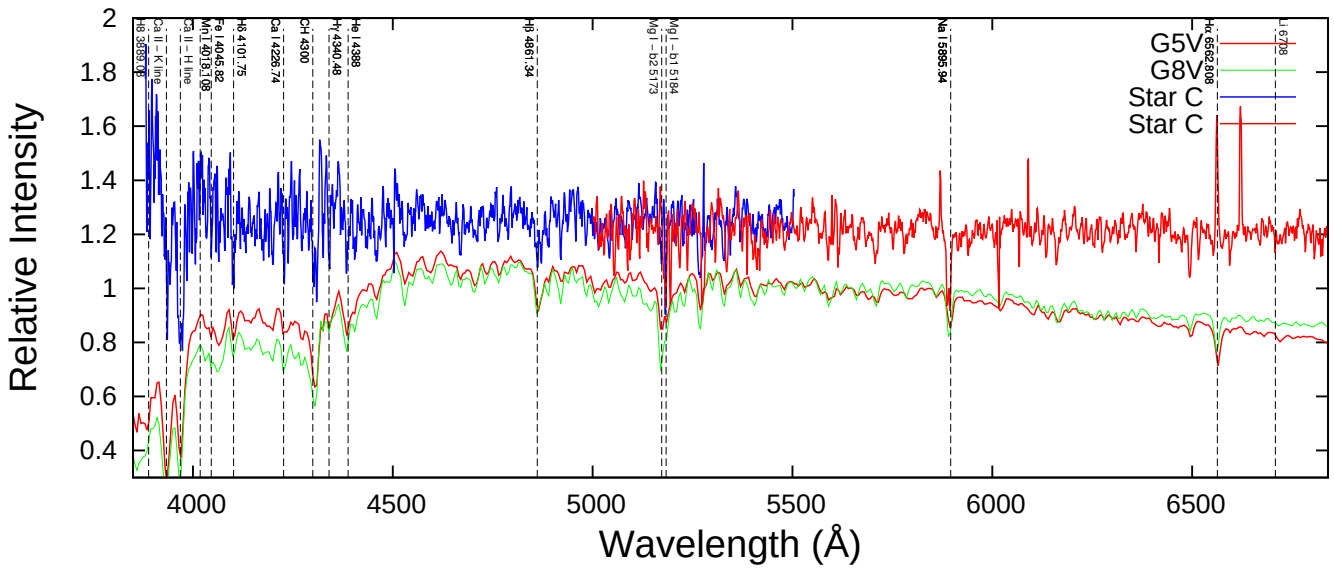

Figure 4.3: The spectral emission profile for star C.

by R.O. Gray (http://ned.ipac.caltech.edu/level5/Gray/frames.html), which has the entire normalised MK-library, was used. The MK-spectral system is a standardised library based on the strength of absorption lines and the masses of stars. It was originally published by Morgan et al. (1943). Stars C and D were classified by measuring the strength of the absorption lines relative to each other. They are low mass stars because of the weak absorption lines that are found in early K type stars.

The strong H and K Ca-II absorption lines in star C along with the rich collection of metal absorption lines (eg. Fe I and the Mg-I b2) suggest an early G type star. Another feature that suggests an early G type star is the Mg-I b1 absorption line that is roughly the same strength as the Na-I

absorption line. In late G type stars the Mg-I line becomes stronger than the Na-I line.

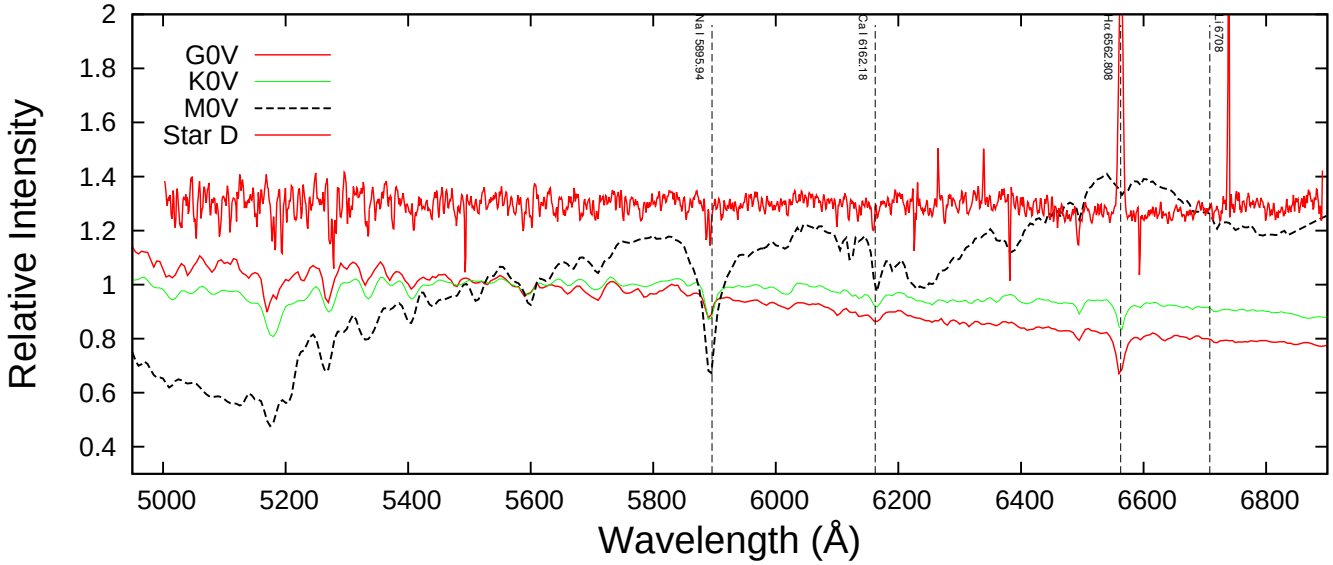

Figure 4.4: The spectral emission profile for star D.

For star D only the red part of the spectrum was available. The spectrum is very similar to that of star C. The rich collection of absorption lines that are roughly of the same strength suggests a late G or K type star. The Fe I ($\lambda \approx 5270$Å) line is stronger than the Na I ($\lambda \approx 5896$Å) line which can be seen in the spectra of the G type star, and not in lower mass stars. Star D therefore seems to be of a spectral type between G and K.

The Na-I (6730 Å) emission line is strong in star C, while the S-II line (6730Å) is strong for star D. In each case the emission line is stronger than the Hα emission line and may originate from circumstellar matter or gas contamination.

The SEDs of T Tauri stars here many types of emission lines, as shown in Fig 2.4. There are many absorption lines and a few emission lines in star C's and D's SEDs, and analysis of the high number of absorption lines falls beyond the scope of this study. This is a general phenomenon in the SED of a T Tauri star. One should keep in mind that each T Tauri's SED is unique and that the emission/absorption lines do vary greatly from star to star. For examples on the different types of SEDs of T Tauri see Hartigan et al. (1991), Hartman (1998), Basri & Bertout (1989) and Basri & Batalha (1990).

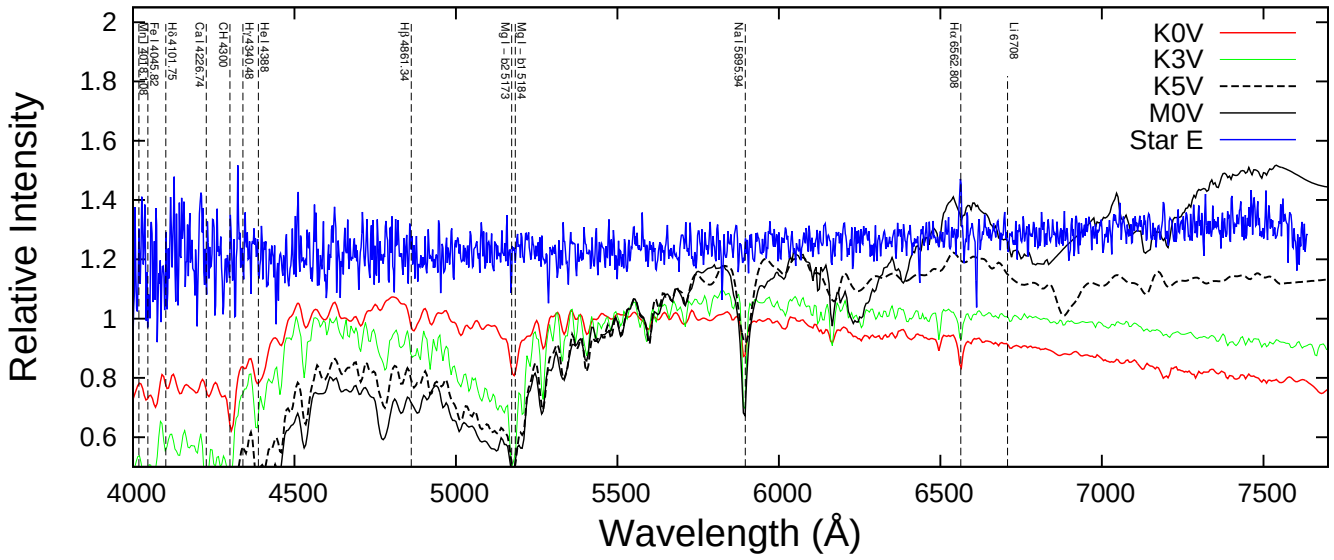

Figure 4.5: The spectral emission profile for star E.

Star E has a very noisy SED, as shown in Fig 4.5. The continuum is very flat and noisy making it very difficult to distinguish between the noise and emission/absorption features. Star E is a 14th magnitude star, as mentioned in Table 4.2, so it would be expected that the spectral profiles would be more prominent in its SED than those of the other stars, unless it has an accretion disk that renders the absorption and emission lines indistinguishable from the continuum. This is not uncommon, and many T Tauri stars have shown similar flat, featureless continuums by Dahm & Simon (2005).

The equivalent width of the Hα emission line was measured for stars A, B and E with the spectroscopic analysis tool **Specview** that was developed by the **S**pace **T**elescope **SC**ience **I**nstitute. The equivalent widths of the Hα line in star A, B and E are respectively 3.8 Å, 16.9 Å and 5.2 Å. Each value was determined by measuring the emission line and the noise towards the long and short wavelength sides. The equivalent widths of the Hα for star C and D were not measured because the software can not handle relative fluxes. If one uses the 10 Å definition for a weak and classical T Tauri, it seems that stars A and E are most probably WTTs and that star B is a CTT.

In a study by Hartigan et al. (1991) the optical excess emission from the accretion disk in a T Tauri star which causes the absorption lines present in photospheric emission to become weak or indistinguishable from the continuum, was called **veiling**. The star that showed the strongest veiling in their study is DR Tau, which has a flat, almost featureless continuum. The continuum for a veiled star is usually so different from an unveiled spectral profile that it may be classified as two spectral types earlier than that of the central star. Hartigan et al. (1991) also found that, out of a population of 22 stars, the excess emission in many revealed a flat continuum from 4000 Å to 8000 Å.

The veiling increases the emission of the star/disk system from 4500 Å to 8000 Å and increases the emission at shorter wavelengths in K type stars. If a K star is not veiled it will have a drastic decrease

in flux at wavelengths shorter than 4500 Å. Star A has a continuum that is flat between 4000 Å and 4500 Å and then increases up to 7500 Å after which it decreases towards the longer wavelengths. In star B's case the continuum has the shape expected of a low mass star. The continuum emission of stars C and D cannot be inspected for increased emission because they are normalised. For star E its continuum stays constant from 4000Å to 4500 Å and then increases slightly towards longer wavelengths. Stars A, B and E all display a significant lack of absorption lines, for example the Na-I line at λ = 5895.94 Å which is seen in all of the considered MS spectral types.

The lack of these absorption lines is evidence of veiling caused by matter moving in tubules from the accretion disk and shocking onto the stellar surface. Gahm et al. (2008) studied T Tauri stars for which the veiling was very strong and found it very difficult to separate the disk's emission from a star/disk system. To correctly deredden a star the exact amount of emission from the disk should be known and how much it veils the star's spectral profile. To calculate by how much the spectra are veiled, it needs to be observed at different time lapses. This technique is beyond the scope of this study.

The spectrum of star C is rich in absorption lines. The Na-I absorption line is strong,which is not the case for the other four stars. The Hα emission line is not as wide as seen in star D. Inspection of the spectrum of star D shows that it is poor in absorption lines but has a very strong Hα emission line. This lack of absorption lines, and the very strong Hα line, may be used to argue that star D's spectrum is most probably veiled by strong emission from an accretion disk.

Comparing the spectra and other features of C and D with the SEDs of stars A, B and E, one may postulate that star C may be a WTT and star D a CTT. Without measuring the equivalent line widths for the Hα emission line one cannot say for certain what type of T Tauri stars C and D are in terms of the 10 Å line width definition for distinction between CTTs and WTTs.

The spectral classification based on the strength of absorption lines relative to each other is probably incorrect due to the influence of veiling on the line strengths. This crude classification was done just to get an idea of the spectral classes of the stars, and to see whether it is in agreement with previous results for T Tauri stars.

Star	α	δ	V	R	I	J	H	K	Spectral type	Av
1 (2011) - A	134.12995	-43.13253		16.2610 ± 0.007	14.605 ± 0.002	12.23 ± 0.013	10.827 ± 0.015	10.207 ± 0.021	K5	
4 (2011) - B	134.13064	-43.13010		14.708 ± 0.005	13.591 ± 0.002	12.107 ± 0.011	11.079 ± 0.014	10.284 ± 0.018	K5-M5	
16 (2002) - C	134.14388	-43.13210	17.295 ± 0.014	16.273 ± 0.005	16.873 ± 0.002	12.230 ± 0.013	10.827 ± 0.015	10.207 ± 0.021	K5	
17 (2002) - D	134.18314	-43.11771	17.640 ± 0.007	16.776 ± 0.008	17.343 ± 0.002	13.011 ± 0.0130	11.699 ± 0.006	11.253 ± 0.014	G-K	4.77
3 (2011) - E	134.16750	-43.15455	16.419 ± 0.013	14.802 ± 0.013	13.775 ± 0.003	12.419 ± 0.012	11.506 ± 0.009	11.17 ± 0.017	K0-K5	0.95

Table 4.2: Summary of the stars that displayed Hα emission.

The properties of the stars that displayed Hα emission lines are given in Table 4.2. Star B is bright in comparison with the other candidate stars. Having an R magnitude of 14 its continuum cannot be contaminated by background noise. This single confirmed CTT allows one to suspect that the region must have more CTTs. The sensitivity limit of the equipment used hindered the possibility of

discovering more CTTs.

Many of the spectra shown in appendices D and E also have flat, almost featureless continuums. This suggests that the majority of these stars may be veiled TTs. Another possibility is that a few of the stars were too faint for the 1.9-m telescope to get a proper $\frac{S}{N}$, signal to noise ratio resulting in a spectral profile of mostly noise. Star 55 in appendix E displays two SEDs. These may be two stars that were caught in the slit. Out of the 38 SEDs that are shown in appendix E, there is only one that has a continuum with the shape expected of a star that may be in the early G spectral class. This is star number 10, a possible field star.

4.2.3 The location of the stars that showed Hα emission lines

The locations of the five stars that each showed an Hα emission line are given in Fig 4.6. A detailed spectral emission profile of each star is given in Figs 4.1 - 4.5. The two Hα emission stars that were discovered in the data set from 2002 are shown in Figs 4.3 and 4.4. These could not be flux calibrated, because there were no standard star data available for this observation run. The other three were flux calibrated, making it possible to aquire a shape for the continuum.

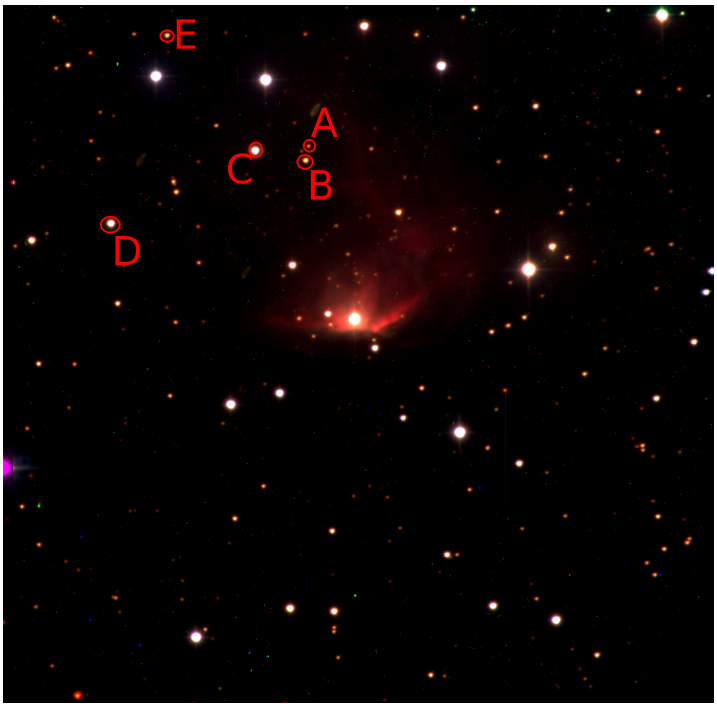

Figure 4.6: The two stars that were observered in 2002 and showed Hα emission are stars C and D. The other stars that showed Hα emission were discovered from the observations taken in 2011. North is at the top of this image.

In Fig 4.6 the direction from the top to the bottom is from South to North and from the left to the right is from West to East. The stars that showed Hα emission lines all lie in the South-Western

quadrant. This quadrant is surrounded by an arch of ionised hydrogen gas and molecular gas. This arch is described by Bik et al. (2010) as a part of the molecular cloud that has been cleared out by the exciting star and is mostly free of molecular gas. Van der Walt et al. (2012) find that a population of young bright objects cluster in this clearing, so this would be the most probable place to find T Tauri stars.

The spectrograph with which the observations were done in 2011 was set up to the slit parallel with the East to West direction. So for stars A and B, which lie very close to each other, careful precautions were taken not to contaminate either of the stars' observations with the other. It is possible that some of the stars in the study may have been contaminated from emission by the HII gas. This cannot be said with certainty but in the reduction process described in chapter 3, during the sky subtraction any emission from gas that could contaminate the emission from the star would be subtracted. However there is a possibility that emission from excited gas could still be present in the spectral profile from the star.

One shortcoming of the spectroscopic observations is that the two stars that showed Hα emission from the 2002 data set were not observed in 2011. This would make it possible to flux calibrate them and see if either shows signs of veiling in their continuum. Another shortcoming of the equipment that was used for the observations in 2011 was the lack of a grating with a resolution higher than 5 Å. This played a very negative role in the quality of the spectra. The biggest shortcoming was the lack of standard star data for the data set in 2002.

The colours and magnitudes of each star that showed Hα emission and was detectable in a filter set are shown on the colour-magnitude and colour-colour magnitude diagrams.

4.3 Photometric results

4.3.1 Introduction

There were 78 stars that matched in the V, R and I filters, 214 in the R and I filters, and 252 stars were detected in the I filter. Colour-colour and colour-magnitude diagrams are presented and discussed for the sources that matched in V, R and I. A colour-magnitude diagram is presented for the sources that matched in R and I.

In the colour-magnitude diagrams, the optical results are tested against data for MS, giant and super-giant stars. Using a $V-R$ against $R-I$ two-colour diagram, stars were dereddened onto the main sequence to calculate the visual extinction for each star. This was used in colour-magnitude diagrams and to calculate an average value for the visual extinction across the field of view. Maps for the location of the sources that matched in the different filters are presented and discussed.

4.3.2 Main sequence, giant and super giant stars

The standard tool to classify **MS** stars according to their masses in terms of their colours and absolute magnitudes is the characteristic spectral type. Standardised optical data for the MS used in this study was found in Allen (1999) and in the NIR is that from Koornneef (1983). The colours and absolute magnitudes of the MS, giants and super giants that were used are given in Tables 4.3a, 4.3b and 4.4 respectively.

Type	V	$V-R$	$R-I$	$V-K$	$J-K$	$H-K$
O5	-5.70	-0.15	-0.32			
O9	-4.50	-0.15	-0.32	-0.89	-0.19	-0.05
B0	-4.00	-0.13	-0.29	-0.85	-0.17	-0.05
B2	-2.45	-0.10	-0.22	-0.67	-0.13	-0.04
B5	-1.20	-0.06	-0.16	-0.43	-0.08	-0.02
B8	-0.25	-0.02	-0.10	-0.25	-0.04	-0.01
A0	0.65	0.02	-0.02	0.00	0.01	0.00
A2	1.30	0.08	0.01	0.13	0.04	0.01
A5	1.95	0.16	0.06	0.35	0.09	0.02
F0	2.70	0.30	0.17	0.79	0.20	0.04
F2	3.60	0.35	0.20	0.93	0.24	0.05
F5	3.50	0.40	0.24	1.01	0.26	0.06
F8	4.00	0.47	0.29	1.12	0.29	0.06
G0	4.40	0.50	0.31	1.22	0.31	0.07
G2	4.70	0.53	0.33	1.49	0.37	0.08
G5	5.10	0.54	0.35			
G8	5.50	0.58	0.38	1.60	0.41	0.09
K0	5.90	0.64	0.42	1.75	0.47	0.10
K2	6.40	0.74	0.48	2.25	0.62	0.13
K5	7.35	0.99	0.63	3.00	0.77	0.16
M0	8.80	1.28	0.91	3.25	0.83	0.18
M2	9.90	1.50	1.19	3.75	0.89	0.21
M5	12.30	1.80	1.67	4.50	0.90	0.29

Table 4.3a: Main sequence stars

Type	V	$V-R$	$R-I$	$V-K$	$J-K$	$H-K$
G5	0.90	0.69	0.48			
G8	0.80	0.70	0.48	2.16	0.59	0.12
K0	0.70	0.77	0.53	2.35	0.64	0.13
K2	0.50	0.84	0.58	2.59	0.72	0.14
K5	-0.20	1.20	0.90	3.67	0.96	0.20
M0	-0.40	1.23	0.94	3.74	0.97	0.21
M2	-0.60	1.34	1.10	4.16	1.04	0.23
M5	-0.30	2.18	1.96	6.20	1.24	0.31

Table 4.3b: Giant stars

Type	V	$V-R$	$R-I$	$V-K$	$J-K$	$H-K$
O9	-6.50	-0.15	-0.32	-0.82	-0.13	0.06
B2	-6.40	-0.05	-0.15	-0.40	-0.07	-0.03
B5	-6.20	0.02	-0.07	-0.13	0.00	-0.01
B8	-6.2	0.02	0.00	0.04	0.05	0.00
A0	-6.30	0.03	0.05	0.21	0.09	0.01
A2	-6.50	0.07	0.07	0.31	0.11	0.02
A5	-6.60	0.12	0.13	0.36	0.12	0.02
F0	-6.60	0.21	0.2	0.63	0.18	0.03
F2	-6.60	0.26	0.21	0.75	0.22	0.04
F5	-6.60	0.35	0.23	0.93	0.27	0.05
F8	-6.50	0.45	0.27	1.21	0.35	0.07
G0	-6.40	0.51	0.33	1.44	0.41	0.08
G2	-6.30	0.58	0.40			
G5	-6.20	0.67	0.44			
G8	-6.10	0.69	0.46	1.99	0.54	0.11
K0	-6.00	0.76	0.48	2.16	0.58	0.12
K2	-5.90	0.85	0.55	2.44	0.65	0.13
K5	-5.80	1.20	0.90	2.72	0.96	0.20
M0	-5.60	1.23	0.94	3.82	0.99	0.21
M2	-5.60	1.34	1.10	4.31	1.06	0.25
M5	-5.60	2.18	1.96	6.30	1.30	0.32

Table 4.4: Super giant stars

4.3.3 Colour-colour and colour-magnitude diagrams

There were 78 stars that matched in the V, R and I filters which were observed with Johnson-Kron filters on DANDICAM. The magnitude for these stars are given in Tables 4.5 and 4.6.

Numbers 14 and 62 in Tables 4.5 and 4.6 were removed from further analysis due to colours that were unrealistic. This can be ascribed to systematic errors. An example of this is saturation of a star on one of the images that was used in the stacking of the master image from which measurements were taken.

DANDICAM uses a Johnson-Kron filter system, rendering it incompatible with standardised data as given in the Johnson-Cousins filter system. The colours were converted to the Johnson-Cousins colour system using equation 2.13. This third-order relation has a negative implication in that the error on any colour that is converted increases significantly. The errors for each colour were calculated as

$$\delta(V-R)_{\rm JC} = 0.0851\times 3\times\left(\sqrt{\delta V_{\rm JK}^2+\delta R_{\rm JK}^2}\sqrt{\delta V_{\rm JK}^2+\delta R_{\rm JK}^2}\right)^2 - 0.3303\times 2\times\left(\sqrt{\delta V_{\rm JK}^2+\delta R_{\rm JK}^2}\sqrt{\delta V_{\rm JK}^2+\delta R_{\rm JK}^2}\right) + 1.0609\times\sqrt{\delta V_{\rm JK}^2+\delta R_{\rm JK}^2}+0.113 \quad (4.1)$$

$$\delta(R-I)_{\rm JC} = -0.16647\times 3\times\left(\sqrt{\delta R_{\rm JK}^2+\delta I_{\rm JK}^2}\sqrt{\delta R_{\rm JK}^2+\delta I_{\rm JK}^2}\right)^2 + 0.4230\times 2\times\left(\sqrt{\delta R_{\rm JK}^2+\delta I_{\rm JK}^2}\sqrt{\delta R_{\rm JK}^2+\delta I_{\rm JK}^2}\right) + 0.9166\times\sqrt{\delta V_{\rm JK}^2+\delta R_{\rm JK}^2}+0.102 \quad (4.2)$$

$$\delta(V-I)_{\rm JC} = -0.00530\times 3\times\left(\sqrt{\delta V_{\rm JK}^2+\delta I_{\rm JK}^2}\sqrt{\delta V_{\rm JK}^2+\delta I_{\rm JK}^2}\right)^2 + 0.0128\times 2\times\left(\sqrt{\delta V_{\rm JK}^2+\delta I_{\rm JK}^2}\sqrt{\delta V_{\rm JK}^2+\delta I_{\rm JK}^2}\right) + 0.9567\times\sqrt{\delta V_{\rm JK}^2+\delta R_{\rm JK}^2}+0.227\ . \quad (4.3)$$

The converted colours of the 76 sources were plotted in relation to standard MS, giant and super giant stars on the colour-colour diagram in Fig 4.7 and in the colour-magnitude diagrams shown in Figs 4.8, 4.9 and 4.10. In all of the diagrams that follow, the MS is represented by a red dashed line with points on each spectral type. The giants are shown as a dashed brown line and the super giants as a solid green line.

The massive O type stars of the intrinsic colour line lie at the bottom left corner of all four diagrams in Fig 4.7 and the low mass M type stars lie at the opposite end of the line. In each diagram only the MS and giants from Allen (1999) are plotted because the isochrones from the models lie on top o f t he MS.

The colours of a specific spectral type are intrinsic when used on a colour-colour diagram, regardless of its luminosity class. The colours are also independent of age if one uses computer models such as those of Marigo et al. (2008) and Siess et al. (2000) to construct isochrones of 10^6, 10^7 or 10^9 years. An experiment was performed to determine the interstellar extinction for the stars that could be dereddened onto the MS. This was done with the assumption that all of the stars on the colour-colour diagram only produce photospheric emission, with no contribution from circumstellar matter. An *octave* program was written to fit a polynomial through the MS, calculate the intersection of each star's dereddening line with the polynomial, and then determine the visual extinction. The equation for the polynomial is

$$VR(x) = 1.097x^6 + 1.090x^5 - 0.810x^4 - 0.6211x^3 + 0.8228x^2 - 0.3578x + 0.069\ , \quad (4.4)$$

with $x = R-I$ and $VR = V-R$. Of the 76 stars that matched in V, R and I, 57 could be dereddened onto the MS. Their colours and visual extinctions are given in Table 4.7. The average visual extinction calculated from the 57 dereddened stars is $A_V = 1.8$. The other 29 could not be dereddened as these sources fall outside of the region on the graph between dereddening lines that are at the maximum and minimum masses on the MS. These sources are given in Table 4.8.

Using the visual extinctions calculated from the $V-R$ against $R-I$ colour-colour diagram, a com-

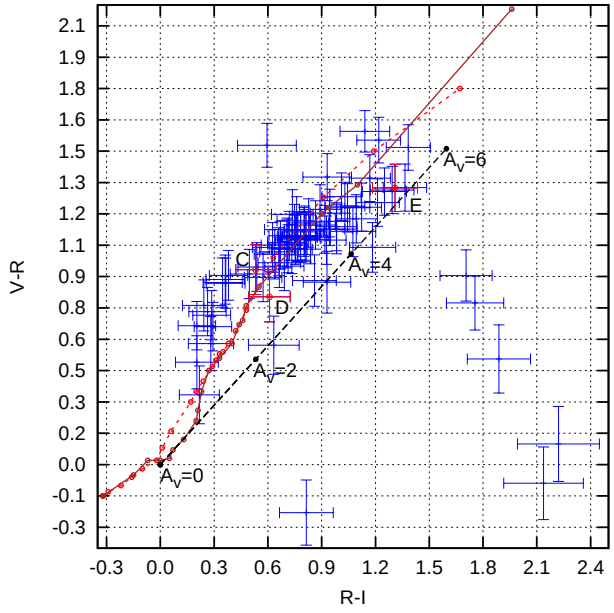

(a)

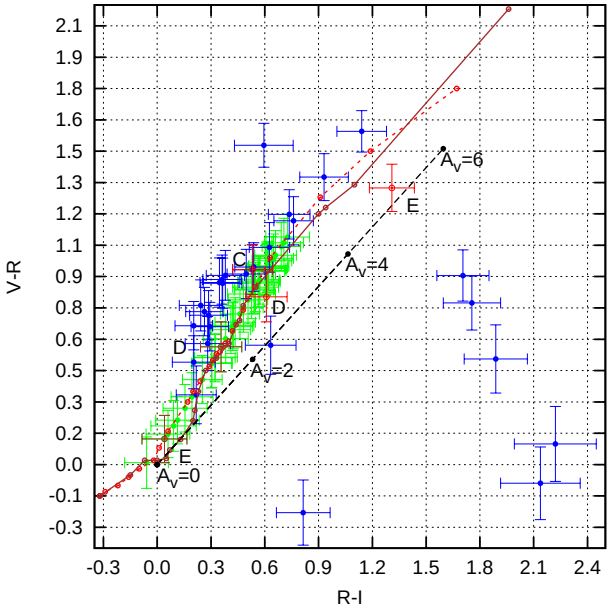

(b)

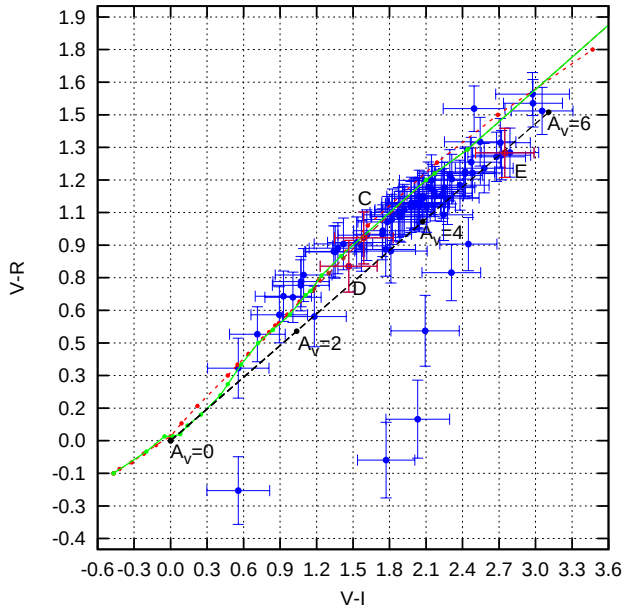

(c) The 76 sources that are displayed in table 4.5 and 4.6

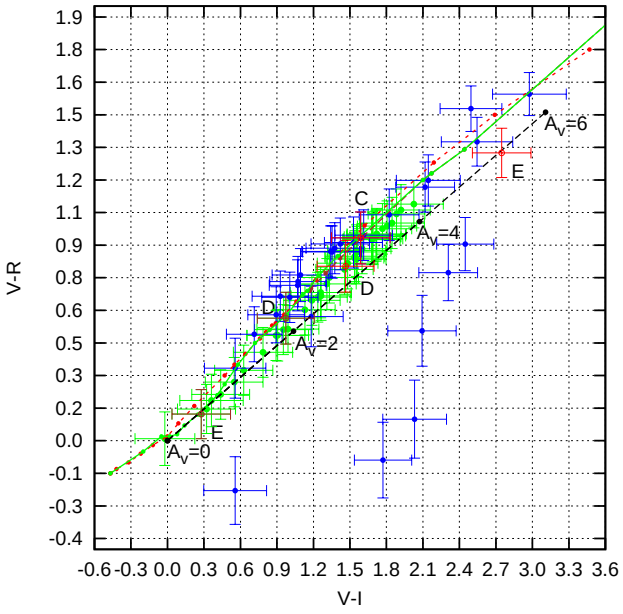

(d) The sources that could be dereddened onto the MS.

Figure 4.7: $V-R$ against $R-I$ colour-colour diagram for the 76 sources that matched in the V, R and I filters. The green datapoints are the sources that could be dereddened onto the MS and the blue datapoints are not dereddened. The red dashed line is the MS from Allen (1999) and the green solid line are the giants.

parison colour-colour diagram was constructed for the $V-R$ and $V-I$ colours to see if the dereddening was correct. In Fig 4.7d the dereddened sources do not lie exactly on the MS as in Fig 4.7b, but the errors of the sources lie within an allowable margin. The reason for using Fig 4.7b to deredden the sources is that the slope of the reddening line in Fig 4.7d is very close to that of the MS, raising the

suspicion that sources that can be dereddened will not be included if Fig 4.7d is used.

The six sources that lay far under the MS cannot be physical, so their incorrect colours have to be systematic errors. This can be due to a star that is on the border of one image and partially on another that was used in the stacking of the master image. If the star was measured with the PSF during data reduction, it would have given the incorrect amount of light.

In Fig 4.7a a grouping can be seen starting from the indicator of star D, under the MS up to the indicator for star E. This group was dereddened onto the MS shown in Fig 4.7b, having colours between $0.01 \leq V - R \leq 1.28$, which is from late K up to early A type stars. This is consistent with the mass range for T Tauri stars.

The same type of grouping was seen in Fig 4.7c as in Fig 4.7a. Fig 4.7d was plotted to check that the dereddening with the *octave* program on the stars in Fig 4.7b is consistent with other colours. The group that was dereddened ranged between early M and early A type stars, quite consistent with that seen in Fig 4.7b. The three stars that showed Hα emission and were detected in the V, R and I filters, were C, D, and E. They are shown in all four diagrams in Fig 4.7 as red crosses. Star D and E could be dereddened but not C as it lies above the MS. The dereddened stars are shown as brown crosses in Figs 4.7b and 4.7d.

The dereddened colours for stars D and E are given in Table 4.9.

Using the dereddened colours in Table 4.9, star D falls between an A0 and A2 type star and star E has colours of between those of an A2 and A5 star. Star C is so close to the MS that one may use this as a pointer as to what stellar type it can be, in the same context as stars D and E. Its colours lie between those of an A2 and an A5 type star.

In Fig 4.8 the colour-magnitude is shown for the sources that matched in the V, R and I filters. Due to the fact that the extinction varies significantly across RCW 34 the positions of the obscured sources are compared with a number of reddened positions for the MS in Fig 4.8a. The MS is plotted with four different visual extinctions: the first is for $A_V = 0$, which is for stars with no extinction. The second is for $A_V = 1.8$ which is the average extinction that was calculated from the stars that were dereddened in Fig 4.7b. The third is $A_V = 4.2$, determined by Heydari-Malayeri (1988). The last one is for $A_V = 5.1$, which was calculated by Van der Walt et al. (2012) for a group of ≈ 700 objects that were only detectable in the NIR and dereddened onto the CTT locus.

In each of the colour-magnitude diagrams in Figs 4.8, 4.9, 4.10 and 4.11 the absolute magnitude is used. The reddening of the MS for the four different extinction coefficients is to demonstrate which one applies best for the population of stars of this study. The normal unreddened MS cannot be used, because the magnitudes in Fig 4.8a have only been corrected for distance and not dereddened for interstellar extinction. The extinction coefficient given by Heydari-Malayeri (1988) is too big because

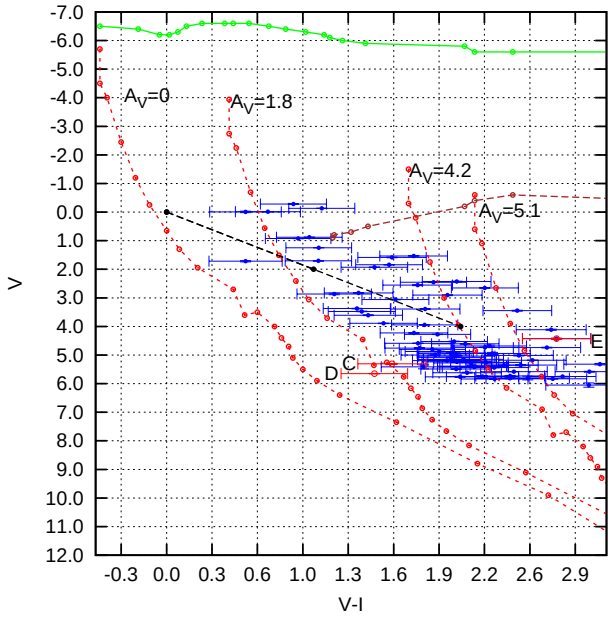

(a) The 76 sources that matched in the V, R and I filters.

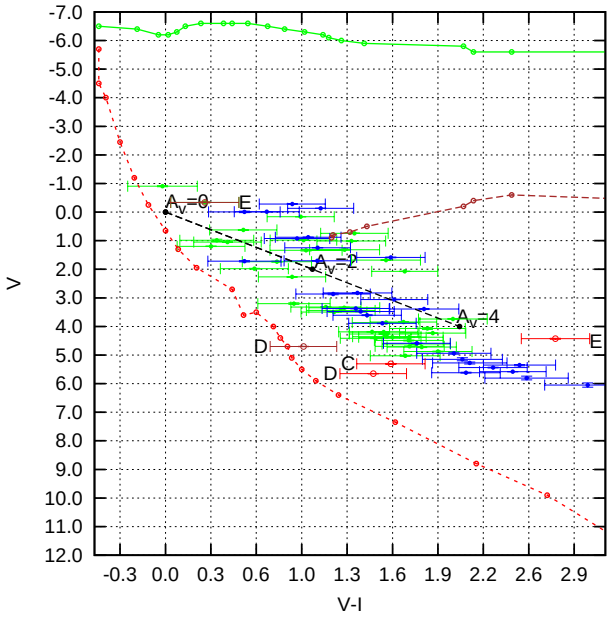

(b) The sources that were dereddened onto the MS branch and those that could not be dereddened.

Figure 4.8: The V against $V - I$ colour-magnitude diagram for the 76 sources that matched in the V, R and I filters.

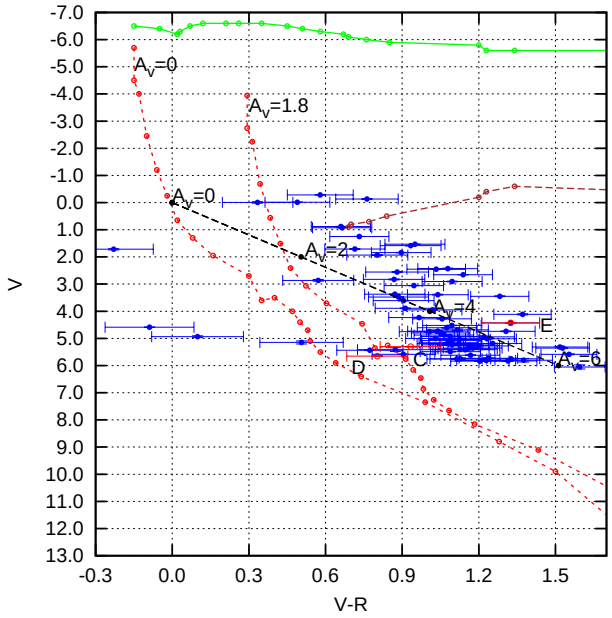

(a) The 76 sources that matched in the V, R and I filters.

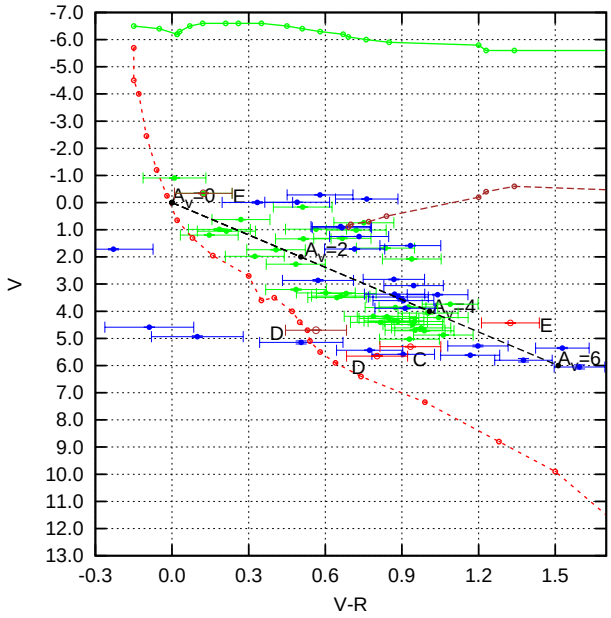

(b) The sources that were dereddened onto the MS and those that could not be dereddened.

Figure 4.9: The V versus $V - R$ colour-magnitude diagram for the 76 sources that matched in the V, R and I filters

the majority of the stars are located on the left of the MS. The extinction coefficient calculated by Van der Walt et al. (2012) to deredden the suspected CTTs onto the empirical T Tauri locus was also too big to use in this study. The reddened MS that best matches the unreddened stars has a visual extinction of $A_V = 1.8$. No sources were detected were dimmer than an absolute magnitude of 6. This is due to the sensitivity limit of the equipment that was used.

In Fig 4.8b the sources that were dereddened in Fig 4.7b are plotted on a colour-magnitude diagram. The grouping seen in the colour-colour diagrams is also seen here, below the reddening line. This group is dispersed in the dereddening onto the MS seen in Fig 4.8b. The group seems to cluster under the dereddening line and between the colours $1.6 \leq V - I \leq 2.6$.

In the dereddened diagram shown in Fig 4.8b, the group is dispersed around the colour-magnitude diagram and above the MS so that they do not cluster anymore. Now if one considers stars C and E that show sign of veiling in their SEDs and are at the opposite ends of the cluster in the colour-colour diagram (Fig 4.7a and the colour-magnitude diagram in Fig 4.8a) the objects may also exhibit veiling. The distribution of the dereddened objects in Fig 4.8b is not on the MS as one would expect from the colour-colour diagram. This implies that the assumption that these stars only exhibit photospheric emission, is incorrect.

If the sources in Fig 4.7a are not just reddened, then their colours have to be affected by something else. By knowing that stars C and E have veiled SEDs and that they are at the opposite ends of the cluster, it may be assumed that these objects are TTs with circumstellar matter that produces optical excess emission adding an extra blue component to the colours. So they may be K-M type stars with brighter $V-R$, $R-I$ and $V-I$ colours than the MS caused by significant amounts of circumstellar matter.

Knowing that the assumption for the dereddening of some of the sources in Fig 4.7b was incorrect, some of the visual extinctions in Table 4.7 also have to be incorrect. Even though this may be the case, the average extinction calculated in the model may still be a good estimation. The reason for this is that the stars that matched in the V, R and I filters are randomly distributed across the field, as shown in Fig 4.12. So in Fig 4.8a, a star that lies above the MS may be reddened or it can be a PMS with a luminosity higher than what its spectral class will have on the MS.

Figs 4.9a and 4.9b are not significantly different to all the previous descriptions. They are included to complement Figs 4.8a and 4.8b and show consistency across different filters.

In Fig 4.10a and 4.10b, the sources that matched in the V, R and I filters are shown on an R versus $R - I$ diagram. The colours and magnitudes of stars A and B, matching amongst the R and I filters, were added additionally even though they were not detected in the V, R and I filters. Here all five the stars that displayed Hα emission are also indicated. Stars C, D and a few other stars in Fig 4.10a are to the left of the MS that is reddened to $A_V = 1.8$. This is not significant if one remembers that the

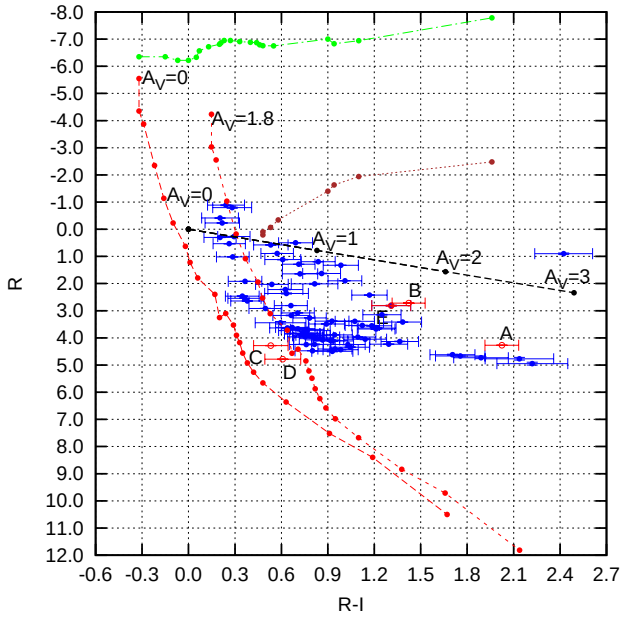

(a) The 76 sources that matched in the V, R and I filters.

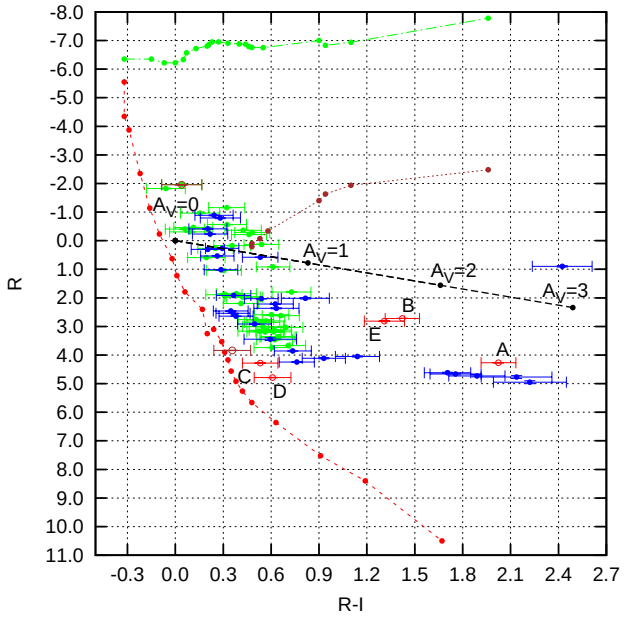

(b) The sources that were dereddened onto the MS branch and those that could not be dereddened.

Figure 4.10: The R versus $R - I$ colour-magnitude diagram for the 76 sources that matched in the V, R and I filters

dereddening may be incorrect.

Clustering can be seen in Fig 4.10a similar to that in Fig 4.8a. In Fig 4.10a the clustered objects are found between the colours $0.6 \leq R - I \leq 1.5$ and between the magnitudes $3.0 \leq R \leq 5.0$. Similar to the V-based colour-magnitude diagrams when they get dereddened, they get dispersed along the MS from early A type stars down to late K type stars. This is all consistent with previous discussions and Fig 4.10 is not significantly different to Figs 4.8 and 4.9.

4.3.4 Sources that only matched in the R and I filters

The stars shown in Fig 4.11, were the ones that all matched in the R and I filters. The stars in this image were not as precisely calibrated as those that matched in the V, R and I filters. This is because the transformation equation (given by equations 3.14 and 3.15) between the instrumental and apparent magnitudes is only dependent on one colour of the linear transformation.

The clustering seen in all of the images for the stars that matched in the V, R and I filters is not so obvious in Fig 4.11. In Fig 4.10a the clustered objects that are pointed out in the section describing Fig 4.10a, end at a magnitude of $R \approx 4.5$. This is most likely caused by a sensitivity limitation for a matching in the V filter. But in Fig 4.11 it seems that this group extends to a magnitude of $R \approx 5.5$. There is a group of objects that extends from $R \approx 5.5$ to the sensitivity limit of $R = 7$. This group may be part of the clustered objects.

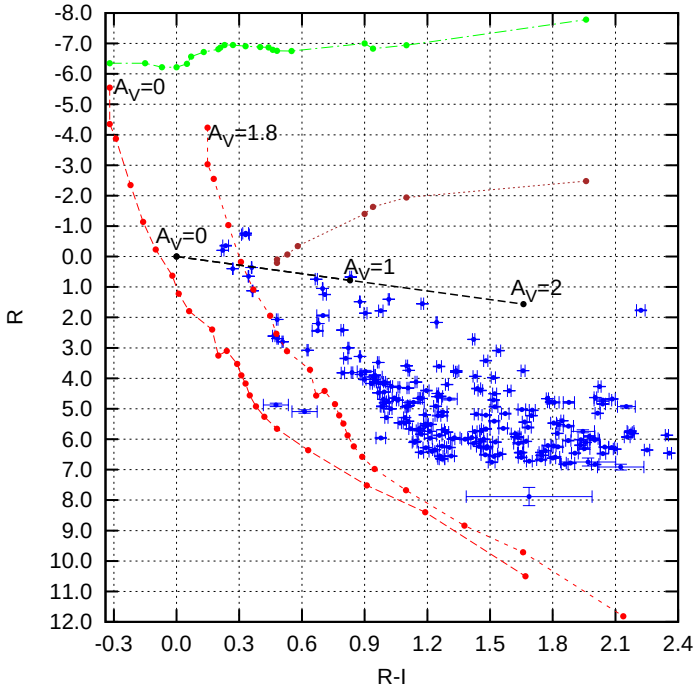

Figure 4.11: The R versus $R-I$ colour-magnitude diagram for the 214 sources that matched in the R and I filters

There are many stars with large $R-I$ colours and faint magnitudes. These can either be very reddened MS stars with a range of a B to F type stars or very young low mass stars. Star A has a colour of $R-I=2.0$ in Fig 4.10a and is not a very reddened star, but a young low mass star which suggests that some of the other objects with these large $R-I$ colours may be young low mass stars.

Fig 4.11 shows the sources that matched in the V, R and I filters and those that only matched in the R and I filters. The figure does show that there are faint embedded objects that were too faint to detect in the V filter. This proves that at longer wavelengths one can detect objects that are more deeply embedded in the molecular cloud. This is consistent with the NIR data that shows that there are many young embedded objects in the region that surrounds RCW 34, but which could not be detected due to the limitations of the equipment used.

In the following section the distribution of the locations of the detected objects is discussed and the NIR colour-colour diagrams are shown and discussed for the sources that matched in the optical and NIR studies.

4.4 Sources that matched in the optical and NIR filters

4.4.1 Correspondence between the coordinates for the optical and near infrared sources

In each of the following images the exciting star of RCW 34 and the masers in the field of view are shown. The exciting star and the stars that showed Hα emission serve as pointers to the position of the stars that are shown in each diagram. Fig 4.6 may be used as a photographic reference for the position of the stars.

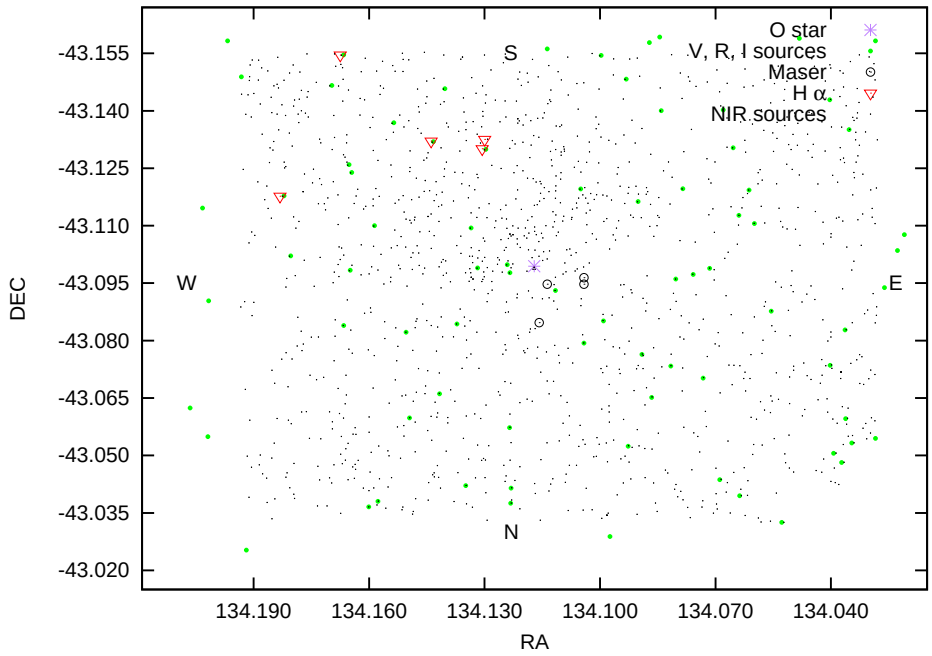

Figure 4.12: The sources that matched in the V, R, I, J, H and K filters

Fig 4.12 shows the sources that matched between the V, R, I, J, H and K filters. The NIR stars are shown as black dots and the optical sources as green dots. DANDICAM's field of view of is larger than that of the IRSF so there are stars that cannot be matched between the optical and NIR images. Only 60 stars matched between the optical and the NIR filters, so 18 optical stars were left out.

The large number of stars that were detected in the NIR study made it easy to confuse sources that are close to each other. The code given in appendix C matches the optical and NIR objects up to 0.001″. The coordinate system on the optical photometric images was manually calibrated so, there may be small errors on the coordinates assigned to those stars. The manual calibrations were done by measuring the coordinates of a star on an image from the DSS and calculating a transformation from the pixel coordinates to ICRS coordinates on the image. The position of a star that was detected in the optical filters might be mismatched if two stars detected in the NIR lay very close to each other.

The stars detected in the V, R and I are randomly distributed across the field of view, as shown in Fig 4.13. There are no prominent signs of the clustering of objects that was seen in the NIR study.

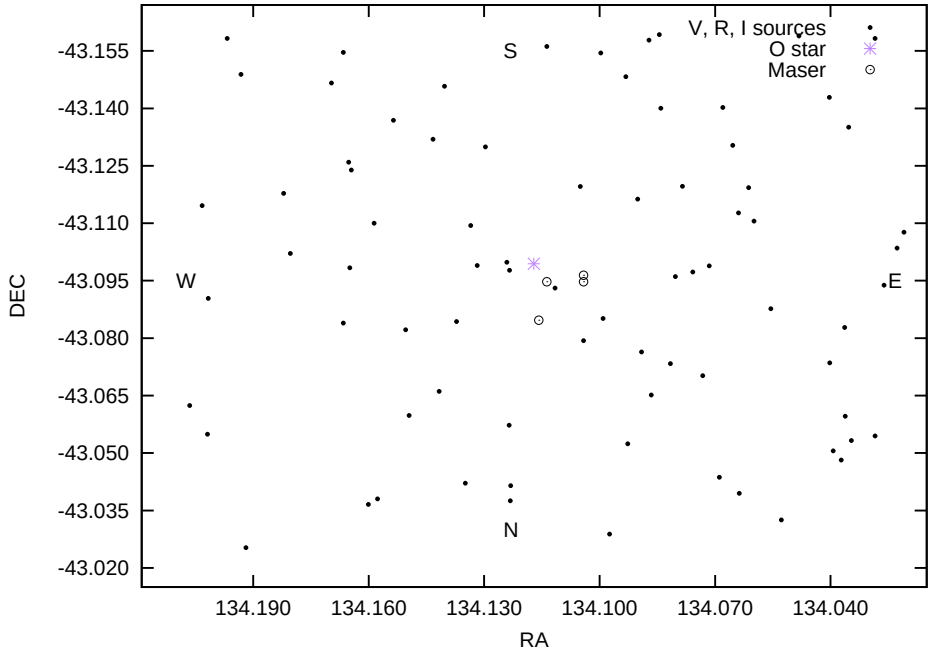

Figure 4.13: Location of the sources that matched in the V, R and I

The random distribution of the stars detected in the optical filters, and the fact that many may have excess blue emission in their colours (shown in Fig 4.7a), suggest that the field is rich in T Tauri stars and that the cluster is bigger than the $7' \times 7'$ field that was studied.

The small number of objects that were detected is due to the limitation of the equipment. With the suggestive proof of possibly two CTTs and three WTTs in the field (the stars with the excess blue emission) and with many stars with possible veiled emission and with the NIR photometric results, there is a good reason to suspect that there may be many more T Tauri stars in the field but they were too obscured to detect in the data for this study.

The sources that matched in the R, I, J, H and K filter filters are shown in Fig 4.14. From the 214 sources that matched in the R and I filters there were 174 that matched with the NIR sources. The significant increase in the number of detected sources makes it possible identify structures more easily than in Fig 4.12.

In Fig 4.15 the sources that matched only in the R and I filters are shown. Clustering from SE of the exciting star to the NW of the star, as described by Van der Walt et al. (2012), is seen here. This clustering does not have the same number of stars as the NIR images do.

Fig 4.15 shows areas clear of stars: one such area right next to the exciting star is caused by the HII region that obscures other stars that may be in this part of the field. The other clear areas are randomly distributed around the image, and may be attributed to parts of the molecular cloud that

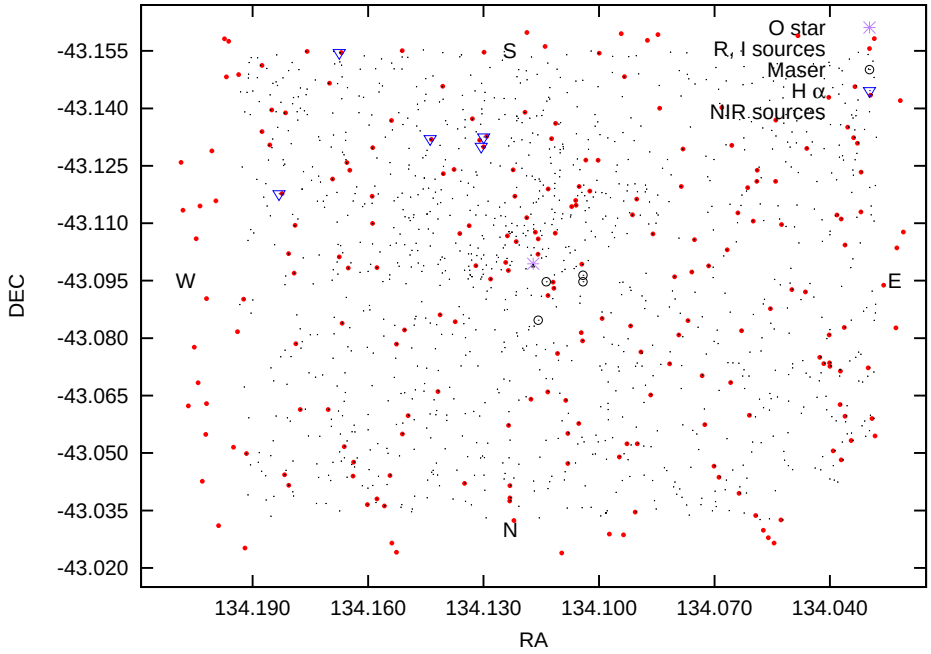

Figure 4.14: The sources that matched in the R, I, J, H and K filters

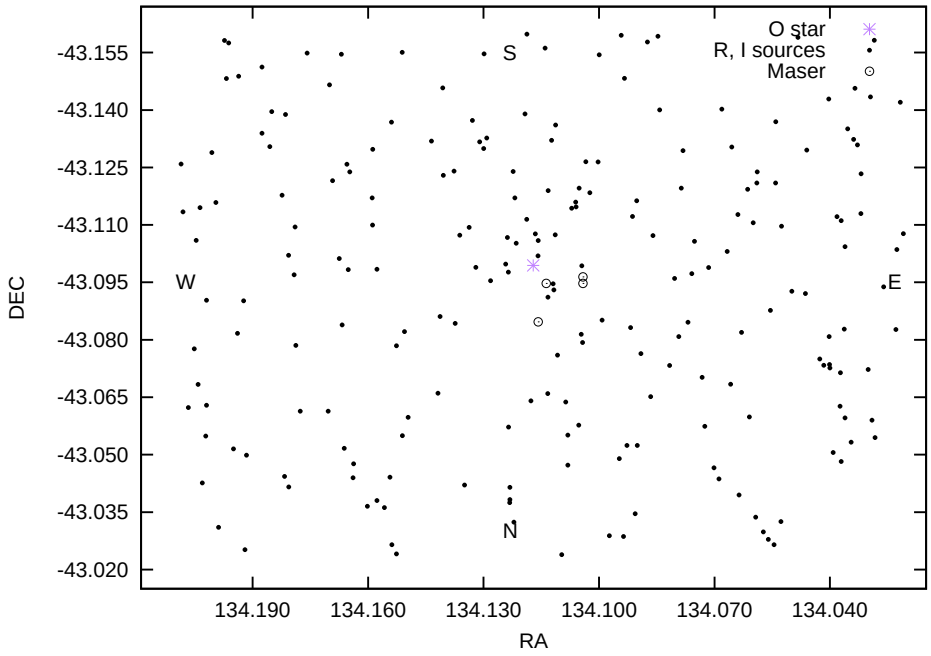

Figure 4.15: Location of the sources that matched in the R and I

are denser than in the areas where the stars are detected.

The increase in the number of sources observed only in the R and I relative to the number observed in the V, R and I may be attributed to extinction that is less for longer wavelengths. The characteristic Hα line is found in the optical R-filter, so it may also be a contributing factor to the increased number of sources that matched up in the $V-$, $R-$ and $I-$filters to only the R and I.

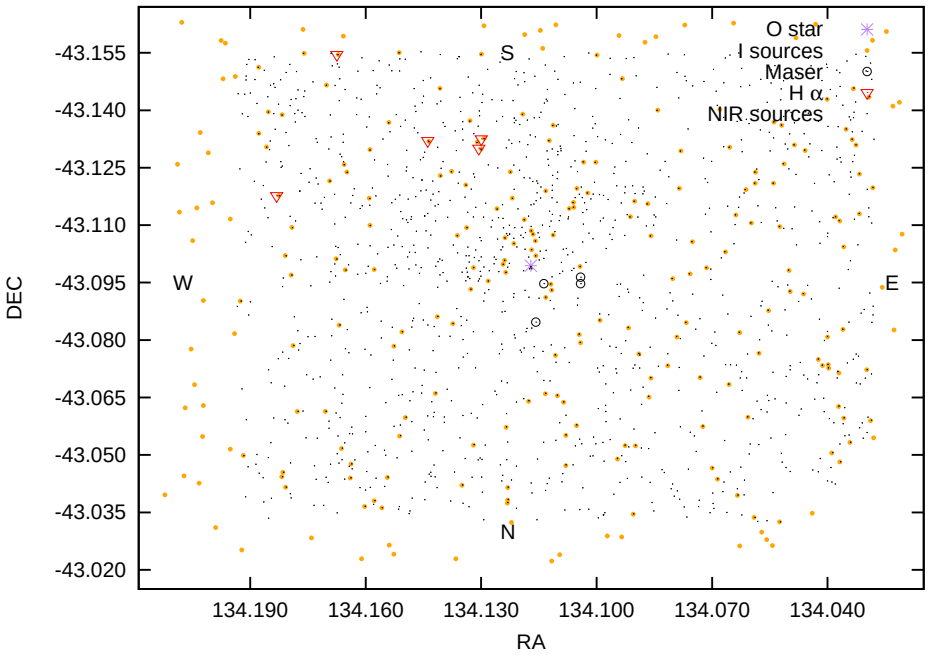

Figure 4.16: The sources that matched in the I, J, H and K filters.

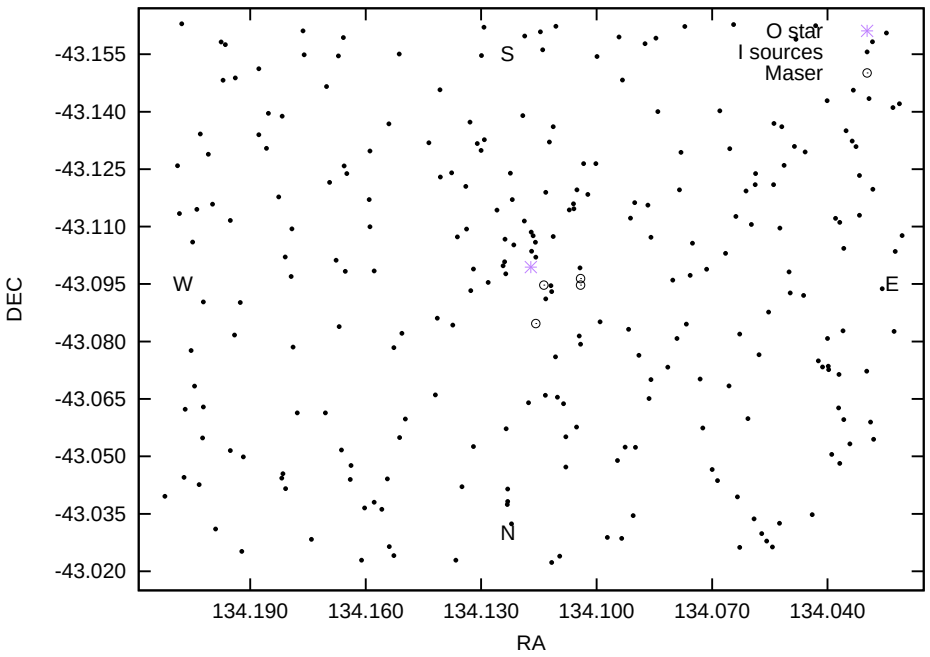

Figure 4.17: Location of the sources that were detected in the I filter.

Fig 4.16 shows many more sources in the NIR than were detected from the I filter. This means that performing an optical study on a region such as this does not yield as many sources as an NIR study does.

The number of sources that were detected only in the I filter is 252, which is not a significant increase in number from the 214 that matched in the R and I filters. The stars that are seen here in the I filter, and not the R, have a uniform distribution across the field, suggesting that the cluster is larger than the field of view for this study. This uniform distribution is consistent with the uniform distribution that was seen in the NIR study by de Villiers (2009).

Using the matched coordinates between the optical and NIR sources, colour-colour diagrams were constructed for the sources that were detected in the different optical filter sets. These diagrams are shown and discussed in the following section. The limited field of view as shown in Figs 4.12, 4.14 and 4.16 should be kept in mind.

4.4.2 NIR colour-colour diagrams

Using the NIR colours from de Villiers (2009) for the sources that matched in the optical and NIR filters $J-H$ versus $H-K$, diagrams were constructed to see where the stars lay relative to the classical T Tauri locus. The interstellar extinction law published by Rieke & Lebofsky (1985) was used to construct the reddening lines.

The T Tauri locus is an empirical line on a $J-H/H-K$ colour-colour diagram, and is caused by the excess NIR emission of T Tauri stars. The equation for the classical T Tauri locus was published by Meyer et al. (1997), and is used as an indicator for T Tauri stars

$$(J-H)_{CTTS} = 0.58 \pm 0.11 \times (H-K)_{CTTS} + 0.52 \pm 0.06 \ . \tag{4.5}$$

Sixty stars matched between the V, R, I and NIR filters. For the R, I and NIR filters there were 174 that matched, and for the I and NIR filters 189 matched.

In each of the of the following colour-colour diagrams, the MS, giant and super giant data from Koornneef (1983) was used. Reddening lines were plotted from the low mass and high mass ends of the MS to provide an indication where reddened field stars may lie. A reddening line was also constructed from the CTT locus and is shown as a blue dashed line in each of the colour-colour diagrams. The equations for the reddening lines are

$$\frac{A_J}{A_V} = 0.282, \ \frac{A_H}{A_V} = 0.175, \ \frac{A_K}{A_V} = 0.112 \ , \tag{4.6}$$

$$E_{J-H} = A_V \times \left(\frac{A_J}{A_V} - \frac{A_H}{A_V} \right) \ , \tag{4.7}$$

$$E_{H-K} = A_V \times \left(\frac{A_H}{A_V} - \frac{A_K}{A_V} \right) \ , \tag{4.8}$$

$$\text{Supergiant reddening line: } (J-H) = \frac{E_{J-H}}{E_{H-K}} \times (H-K) + 0.46 \tag{4.9}$$

$$\text{Main sequence reddening line: } (J-H) = \frac{E_{J-H}}{E_{H-K}} \times (H-K) - 0.21 \tag{4.10}$$

$$\text{T Tauri reddening line: } (J-H) = \frac{E_{J-H}}{E_{H-K}} \times (H-K) - \left(1.1 - \frac{E_{J-H}}{E_{H-K}}\right) \tag{4.11}$$

$$\text{T Tauri locus: } (J-H) = 0.58 \times (H-K) + 0.52\ . \tag{4.12}$$

In Fig 4.18 the 60 sources that matched in the V, R, I, J, H and K filter are shown. The red dots are the NIR data points, the MS is the solid black line and the giants are denoted by the red solid line. Similarly for the R, I, J, H and K filters there were 174 sources that matched up, and are shown on the left side of Fig 4.14. There were 189 sources that matched up in the I, J, H and K filters, shown on a colour-colour diagram in the right side of Fig 4.16.

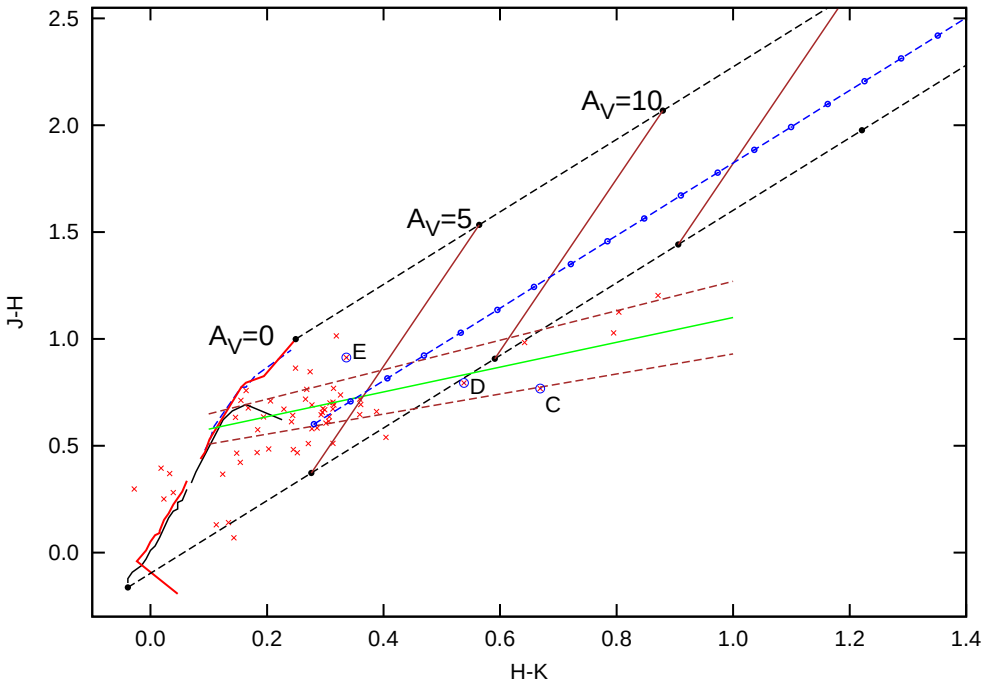

Figure 4.18: Colour-colour diagram for the sources that match up in the V, R, I, J, H and K filters.

Fig 4.18 shows the three stars C, D and E that had Hα emission. They are indicated with a blue circle with a dot at the centre, and their Hα indicators are plotted over their colour indicators. Star C is too far away from the reddening line of the high mass end of the MS to safely state that it may be a reddened high-mass star. It lies on the lower limit of the classical T Tauri locus, meaning that it does not have as much excess emission as other stars shown in the study by de Villiers (2009). The position of star C on the optical colour-colour diagram in Fig 4.7a is above the MS. Its spectrum in Fig 4.3 suggests that it may be a WTT star. The low excess NIR emission, the optical spectral profile

and the the optical colours indicate that star C is a WTT.

Star D lies close to the intersection of the high-mass reddening line of the MS and the CTT locus. The spectra of star D (shown in Fig 4.4) is highly veiled and its optical colours are bluer than those of the intrinsic colour line. So star D cannot be a reddened high-mass star, but is most likely a CTT. Even if star D was a massive star one would expect to see strong Hα absorption.

Star E lies in a region of the colour-colour diagram where mature WTTs are usually found between the low mass end of the MS and the CTT locus. Its Hα equivalent line width of 5.2 Å that was measured from the SED shown in Fig 4.5, also suggests that it may be a WTT. In Fig 4.7a it lies far from the MS, and therefore it may be a highly reddened WTT.

The majority of the stars in Fig 4.18 lie close to the MS, and may be reddened field stars. Only six stars lie between the lower limit of the CTT locus and the reddening line of the high mass end of the MS. Stars C and D being amongst these six suggests that the other four may also be the TTs.

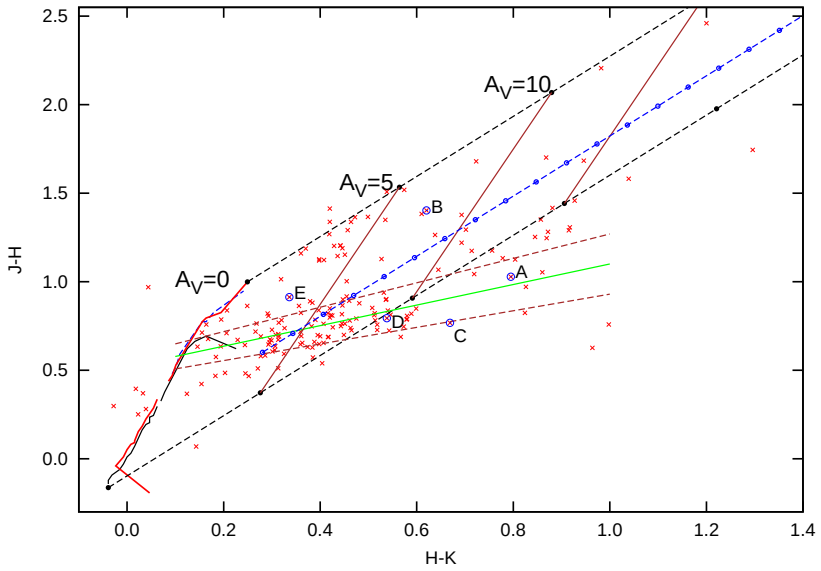

Figure 4.19: Colour-colour diagram for the 174 sources that match up in the *R*, *I*, *J*, *H* and *K* filters.

In Fig 4.19 the 174 stars that matched between the *R*, *I*, *J*, *H* and *K* filters are shown. The majority of the stars seem to gather between the upper and lower limits of the CTT locus, the reddening lines of the TT locus and the high-mass end of the MS. This is not the same type of clustering that was seen at the far end of the CTT locus by de Villiers (2009). Not many stars are seen at the far-end of the locus, which means that if there are CTTs in the cluster that have strong Hα emission they are too far embedded in the molecular cloud.

Star A lies very close to the CTT locus and the strong excess emission that it exhibits places it in

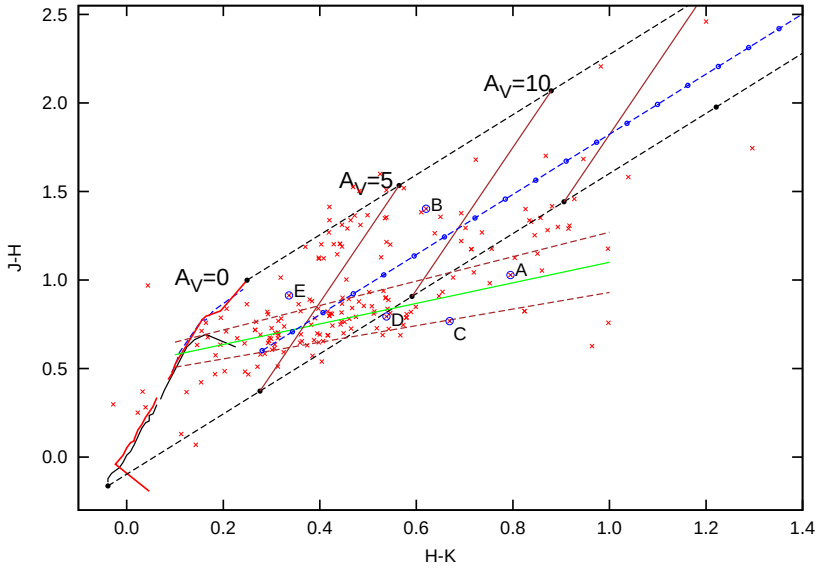

Figure 4.20: Colour-colour diagram for the 189 sources that match up in the I, J, H and K filters.

a region of the diagram where one would most probably find CTTs. Star A's equivalent line width for the Hα emission line is 16.9 Å and it's SED in Fig 4.1 is highly veiled, which is complementory to the NIR data and strongly suggests that star A is a CTT.

Star B lies in a region of Fig 4.19 where it may be a highly reddened WTT. Its SED in 4.2 is not as veiled as that of A and its Hα emission line's equivalent width is 5.2 Å, suggesting that it is a WTT. With a SED that is characteristic of a WTT and a position close to the low mass end of the MS, it has to be a reddened low-mass WTT.

Fig 4.20 shows the 189 stars that matched between the I, J, H and K filters. In this image not much more can be seen than in Fig 4.19.

ID	α	δ	V	δV	R	δR	I	δI
vri-1	134.1427	-43.06612	17.395	0.004	16.087	0.005	15.368	0.003
vri-2	134.0901	-43.07641	11.858	0.003	11.103	0.016	10.959	0.005
vri-3	134.1676	-43.08394	17.346	0.012	15.959	0.009	15.102	0.002
vri-4	134.0664	-43.13035	17.402	0.014	16.061	0.005	15.383	0.003
vri-5	134.1413	-43.14579	11.706	0.004	11.196	0.022	11.014	0.004
vri-6	134.1942	-43.14888	16.719	0.011	15.547	0.015	14.619	0.005
vri-7	134.1007	-43.15444	17.173	0.007	15.664	0.008	14.714	0.008
vri-8	134.0882	-43.15780	17.573	0.007	16.609	0.021	15.255	0.003
vri-9	134.0984	-43.02886	16.513	0.007	15.254	0.003	14.643	0.003
vri-10	134.0538	-43.03255	16.266	0.006	15.068	0.003	14.519	0.002
vri-11	134.1359	-43.04211	13.831	0.008	12.880	0.002	12.440	0.001
vri-12	134.0403	-43.05055	17.750	0.018	16.461	0.006	15.835	0.004
vri-13	134.1245	-43.05724	15.938	0.006	14.799	0.003	14.286	0.002
vri-14	134.1244	-43.09770	17.343	0.023	15.432	0.046	14.974	0.013
vri-15	134.1659	-43.09835	17.739	0.008	16.120	0.010	15.049	0.003
vri-16	134.0851	-43.14005	16.789	0.005	15.600	0.003	15.080	0.003
vri-17	134.1707	-43.14663	11.976	0.002	11.576	0.017	11.470	0.001
vri-18	134.1147	-43.15618	13.523	0.011	12.490	0.005	11.952	0.002
vri-19	134.1978	-43.15827	17.426	0.012	16.655	0.027	15.257	0.007
vri-20	134.0855	-43.15925	16.578	0.008	16.758	0.051	14.975	0.003
vri-21	134.0647	-43.03946	13.236	0.004	12.523	0.002	12.359	0.001
vri-22	134.1241	-43.04149	14.440	0.006	13.278	0.002	12.723	0.001
vri-23	134.1514	-43.08218	12.870	0.004	12.255	0.002	12.062	0.001
vri-24	134.0565	-43.08769	16.988	0.012	15.830	0.006	15.258	0.006
vri-25	134.1345	-43.10942	14.419	0.015	13.186	0.005	12.530	0.001
vri-26	134.0609	-43.11057	17.181	0.016	15.952	0.006	15.364	0.004
vri-27	134.0623	-43.11931	17.194	0.015	15.893	0.005	15.264	0.004
vri-28	134.0942	-43.14827	12.914	0.004	12.293	0.002	12.187	0.001
vri-29	134.1242	-43.03751	17.737	0.027	16.426	0.007	15.656	0.003
vri-30	134.0382	-43.04819	17.376	0.016	16.020	0.005	15.373	0.004
vri-31	134.0937	-43.05243	15.363	0.010	14.450	0.004	14.207	0.005
vri-32	134.0356	-43.05325	17.071	0.013	15.816	0.005	15.220	0.003
vri-33	134.0294	-43.05445	17.306	0.025	15.409	0.007	14.323	0.009
vri-34	134.0826	-43.07332	17.479	0.014	16.230	0.014	15.594	0.017
vri-35	134.0412	-43.07354	17.247	0.022	15.878	0.006	15.138	0.004
vri-36	134.1052	-43.07932	15.596	0.014	14.631	0.004	14.358	0.002
vri-37	134.1382	-43.08434	13.696	0.007	13.007	0.003	12.821	0.001
vri-38	134.1126	-43.09306	14.817	0.015	13.908	0.005	13.649	0.002
vri-39	134.0768	-43.09729	17.226	0.013	15.967	0.011	15.335	0.014
vri-40	134.1328	-43.09896	17.573	0.014	15.628	0.011	14.673	0.004
vri-41	134.1251	-43.09981	14.894	0.016	13.634	0.007	13.073	0.005
vri-42	134.1814	-43.10211	16.219	0.011	15.161	0.012	14.646	0.003
vri-43	134.1596	-43.11000	17.822	0.011	16.221	0.011	15.207	0.003
vri-44	134.0795	-43.11963	17.147	0.010	15.909	0.004	15.298	0.004
vri-45	134.1655	-43.12390	16.728	0.010	15.138	0.012	14.158	0.002
vri-46	134.1662	-43.12592	17.030	0.020	15.724	0.029	15.140	0.036
vri-47	134.1307	-43.12995	16.103	0.019	14.416	0.007	13.500	0.002
vri-48	134.1443	-43.13193	13.574	0.014	12.567	0.007	12.162	0.002

Table 4.5: The sources that matched in the V, R and I filters.

ID	α	δ	V	δV	R	δR	I	δI
vri-49	134.1676	-43.15462	16.419	0.013	14.802	0.013	13.775	0.003
vri-50	134.0699	-43.04368	17.828	0.008	16.397	0.004	15.656	0.003
vri-51	134.0742	-43.07022	15.046	0.009	14.020	0.002	13.609	0.002
vri-52	134.1001	-43.08514	17.004	0.016	15.529	0.004	14.649	0.003
vri-53	134.0813	-43.09606	16.867	0.013	15.658	0.004	15.107	0.003
vri-54	134.0725	-43.09887	16.921	0.012	15.673	0.004	15.074	0.003
vri-55	134.0649	-43.11269	14.644	0.008	13.316	0.006	12.545	0.004
vri-56	134.0911	-43.11630	17.606	0.014	16.233	0.005	15.639	0.003
vri-57	134.1831	-43.11782	13.919	0.007	13.106	0.010	12.636	0.002
vri-58	134.1060	-43.11962	15.438	0.015	13.886	0.004	13.094	0.002
vri-59	134.0363	-43.13506	17.268	0.035	15.847	0.009	15.273	0.004
vri-60	134.1546	-43.13686	17.800	0.020	16.330	0.014	15.512	0.004
vri-61	134.0690	-43.14023	15.881	0.011	14.906	0.003	14.531	0.002
vri-62	134.1929	-43.02527	17.719	0.089	12.886	0.026	10.581	0.016
vri-63	134.1505	-43.05980	16.599	0.010	15.372	0.004	14.646	0.003
vri-64	134.2075	-43.06240	17.795	0.066	16.101	0.021	15.372	0.006
vri-65	134.0876	-43.06517	17.719	0.015	16.236	0.005	15.429	0.003
vri-66	134.0373	-43.08277	15.465	0.009	14.530	0.004	14.274	0.002
vri-67	134.0492	-43.15892	16.927	0.034	16.940	0.052	15.051	0.005
vri-68	134.2029	-43.05491	18.040	0.074	16.039	0.021	15.145	0.006
vri-69	134.0372	-43.05962	16.744	0.014	15.624	0.006	15.130	0.007
vri-70	134.0271	-43.09380	15.379	0.018	14.207	0.007	13.723	0.004
vri-71	134.0237	-43.10353	14.854	0.029	14.354	0.021	13.864	0.021
vri-72	134.2043	-43.11458	14.545	0.018	13.618	0.013	12.945	0.004
vri-73	134.2027	-43.09039	16.673	0.033	15.380	0.015	14.538	0.003
vri-74	134.0294	-43.15826	17.138	0.054	16.719	0.034	15.198	0.005
vri-75	134.1611	-43.03658	11.982	0.026	11.759	0.009	11.639	0.001
vri-76	134.0413	-43.14285	16.935	0.039	15.477	0.009	14.779	0.003
vri-77	134.0219	-43.10768	13.708	0.023	14.002	0.025	13.365	0.022
vri-78	134.1587	-43.03803	17.403	0.071	16.487	0.019	15.759	0.006

Table 4.6: The sources that matched in the V, R and I filters.

V	δV	R	δR	I	δI	$(V-R)_{dr}$	$\delta(V-R)_{dr}$	$(R-I)_{dr}$	$\delta(R-I)_{dr}$	$(V-I)_{dr}$	$\delta(V-I)_{dr}$	A_V
17.395	0.004	16.087	0.005	15.368	0.003	0.645	0.114	0.410	0.110	2.174	0.232	1.905
17.346	0.012	15.959	0.009	15.102	0.002	0.324	0.115	0.194	0.117	2.378	0.239	3.380
17.402	0.014	16.061	0.005	15.383	0.003	0.840	0.115	0.543	0.110	2.167	0.241	1.214
16.719	0.011	15.547	0.015	14.619	0.005	-0.014	0.118	0.070	0.128	2.243	0.239	4.183
17.173	0.007	15.664	0.008	14.714	0.008	0.213	0.113	0.112	0.121	2.578	0.237	4.131
16.513	0.007	15.254	0.003	14.643	0.003	0.925	0.114	0.602	0.108	2.026	0.234	0.673
16.266	0.006	15.068	0.003	14.519	0.002	1.043	0.114	0.692	0.106	1.909	0.233	0.049
17.750	0.018	16.461	0.006	15.835	0.004	0.929	0.117	0.605	0.112	2.068	0.245	0.732
17.739	0.008	16.120	0.010	15.049	0.003	0.003	0.112	-0.031	0.120	2.789	0.235	5.247
13.523	0.011	12.490	0.005	11.952	0.002	0.751	0.117	0.481	0.109	1.741	0.238	0.790
14.440	0.006	13.278	0.002	12.723	0.001	0.938	0.114	0.612	0.105	1.880	0.233	0.375
16.988	0.012	15.830	0.006	15.258	0.006	0.868	0.117	0.562	0.113	1.892	0.240	0.643
14.419	0.015	13.186	0.005	12.530	0.001	0.721	0.116	0.461	0.109	2.044	0.242	1.417
17.181	0.016	15.952	0.006	15.364	0.004	0.951	0.117	0.622	0.112	1.975	0.243	0.493
17.194	0.015	15.893	0.005	15.264	0.004	0.942	0.116	0.615	0.111	2.083	0.242	0.710
17.737	0.027	16.426	0.007	15.656	0.003	0.485	0.118	0.304	0.113	2.225	0.254	2.549
17.376	0.016	16.020	0.005	15.373	0.004	0.987	0.115	0.649	0.111	2.152	0.243	0.668
17.071	0.013	15.816	0.005	15.220	0.003	0.975	0.116	0.639	0.110	2.008	0.240	0.464
17.306	0.025	15.409	0.007	14.323	0.009	0.514	0.108	0.323	0.122	3.054	0.254	3.983
17.479	0.014	16.230	0.014	15.594	0.017	0.816	0.117	0.526	0.133	2.040	0.249	1.078
17.247	0.022	15.878	0.006	15.138	0.004	0.682	0.116	0.435	0.113	2.251	0.249	1.914
17.226	0.013	15.967	0.011	15.335	0.014	0.849	0.117	0.548	0.127	2.046	0.246	0.975
17.573	0.014	15.628	0.011	14.673	0.004	1.088	0.109	0.727	0.122	2.979	0.241	1.843
16.219	0.011	15.161	0.012	14.646	0.003	0.874	0.118	0.566	0.118	1.742	0.238	0.363
17.822	0.011	16.221	0.011	15.207	0.003	0.146	0.113	0.059	0.122	2.721	0.238	4.634
17.147	0.010	15.909	0.004	15.298	0.004	0.883	0.115	0.573	0.110	2.006	0.237	0.785
16.728	0.010	15.138	0.012	14.158	0.002	0.269	0.113	0.155	0.123	2.680	0.237	4.115
16.103	0.019	14.416	0.007	13.500	0.002	0.666	0.112	0.424	0.114	2.710	0.246	2.796
16.419	0.013	14.802	0.013	13.775	0.003	0.122	0.113	0.040	0.125	2.748	0.240	4.770
17.828	0.008	16.397	0.004	15.656	0.003	0.788	0.114	0.506	0.109	2.311	0.235	1.650
17.004	0.016	15.529	0.004	14.649	0.003	0.406	0.114	0.251	0.110	2.481	0.243	3.275
16.867	0.013	15.658	0.004	15.107	0.003	1.062	0.116	0.706	0.108	1.921	0.240	0.003
16.921	0.012	15.673	0.004	15.074	0.003	0.948	0.116	0.619	0.109	2.004	0.239	0.553
14.644	0.008	13.316	0.006	12.545	0.004	0.511	0.114	0.321	0.113	2.242	0.236	2.489
13.919	0.007	13.106	0.010	12.636	0.002	0.563	0.119	0.356	0.115	1.464	0.234	0.948
15.438	0.015	13.886	0.004	13.094	0.002	0.835	0.113	0.539	0.109	2.471	0.242	1.771
17.800	0.020	16.330	0.014	15.512	0.004	0.602	0.115	0.382	0.125	2.419	0.247	2.487
16.599	0.010	15.372	0.004	14.646	0.003	0.484	0.115	0.303	0.109	2.104	0.237	2.341
17.719	0.015	16.236	0.005	15.429	0.003	0.660	0.114	0.420	0.111	2.421	0.242	2.289
14.545	0.018	13.618	0.013	12.945	0.004	0.009	0.123	-0.059	0.122	1.768	0.245	3.456
16.673	0.033	15.380	0.015	14.538	0.003	0.185	0.121	0.091	0.126	2.276	0.260	3.695
16.935	0.039	15.477	0.009	14.779	0.003	1.002	0.117	0.660	0.116	2.296	0.266	0.869
17.403	0.071	16.487	0.019	15.759	0.006	-0.003	0.147	0.004	0.132	1.810	0.297	3.477

Table 4.7: The sources that matched in V, R and I that were dereddened onto the MS, with their colours converted to the Johnson-Cousins colours, the colours dereddened to the MS and then their visual extinctions.

V	δV	R	δR	I	δI	$(V-R)_{JC}$	$\delta(V-R)_{JC}$	$(R-I)_{JC}$	$\delta(R-I)_{JC}$	$(V-I)_{JC}$	$\delta(V-I)_{JC}$
11.858	0.003	11.103	0.016	10.959	0.005	0.762	0.122	0.242	0.119	1.093	0.232
11.706	0.004	11.196	0.022	11.014	0.004	0.579	0.129	0.281	0.125	0.893	0.232
17.573	0.007	16.609	0.021	15.255	0.003	0.904	0.122	1.705	0.145	2.447	0.234
17.343	0.023	15.432	0.046	14.974	0.013	1.528	0.105	0.594	0.164	2.494	0.253
11.976	0.002	11.576	0.017	11.470	0.001	0.489	0.126	0.203	0.119	0.713	0.229
17.426	0.012	16.655	0.027	15.257	0.007	0.773	0.129	1.755	0.159	2.308	0.241
16.578	0.008	16.758	0.051	14.975	0.003	-0.089	0.173	2.137	0.221	1.771	0.235
13.236	0.004	12.523	0.002	12.359	0.001	0.732	0.115	0.262	0.104	1.072	0.231
12.870	0.004	12.255	0.002	12.062	0.001	0.660	0.115	0.293	0.104	1.005	0.231
12.914	0.004	12.293	0.002	12.187	0.001	0.664	0.115	0.203	0.104	0.927	0.231
15.363	0.010	14.450	0.004	14.207	0.005	0.871	0.117	0.347	0.109	1.341	0.238
15.596	0.014	14.631	0.004	14.358	0.002	0.905	0.119	0.380	0.107	1.420	0.240
13.696	0.007	13.007	0.003	12.821	0.001	0.714	0.117	0.286	0.105	1.070	0.233
14.817	0.015	13.908	0.005	13.649	0.002	0.868	0.120	0.364	0.108	1.353	0.241
13.574	0.014	12.567	0.007	12.162	0.002	0.933	0.119	0.531	0.111	1.588	0.241
15.046	0.009	14.020	0.002	13.609	0.002	0.945	0.116	0.538	0.105	1.612	0.236
17.606	0.014	16.233	0.005	15.639	0.003	1.167	0.115	0.760	0.110	2.118	0.241
17.268	0.035	15.847	0.009	15.273	0.004	1.197	0.118	0.736	0.115	2.144	0.262
15.881	0.011	14.906	0.003	14.531	0.002	0.912	0.117	0.496	0.106	1.528	0.238
17.719	0.089	12.886	0.026	10.581	0.016	7.132	-0.033	2.423	0.187	5.780	0.323
17.795	0.066	16.101	0.021	15.372	0.006	1.376	0.112	0.930	0.135	2.544	0.294
15.465	0.009	14.530	0.004	14.274	0.002	0.885	0.117	0.361	0.107	1.375	0.236
16.927	0.034	16.940	0.052	15.051	0.005	0.099	0.179	2.220	0.228	2.031	0.261
18.040	0.074	16.039	0.021	15.145	0.006	1.595	0.098	1.140	0.138	2.975	0.302
15.379	0.018	14.207	0.007	13.723	0.004	1.039	0.118	0.625	0.112	1.822	0.245
14.854	0.029	14.354	0.021	13.864	0.021	0.571	0.139	0.6331	0.141	1.181	0.262
17.138	0.054	16.719	0.034	15.198	0.005	0.505	0.163	1.888	0.176	2.092	0.281
11.982	0.026	11.759	0.009	11.639	0.001	0.334	0.138	0.217	0.111	0.556	0.252
13.708	0.023	14.002	0.025	13.365	0.022	-0.229	0.155	0.814	0.150	0.556	0.257

Table 4.8: The sources that matched in V, R and I that could not be dereddened onto the MS, with their colours converted to the Johnson-Cousins colours.

Star	$V-R$	$R-I$	$V-I$
D	0.119 ± 0.356	0.115 ± 1.464	0.234 ± 0.949
E	0.131 ± 0.040	0.126 ± 0.275	0.241 ± 0.477

Table 4.9: The dereddened colours of stars D and E